Enhanced PIP_3 signaling in POMC neurons causes K_{ATP} channel activation and leads to diet-sensitive obesity

Leona Plum,[1,2] Xiaosong Ma,[3] Brigitte Hampel,[1] Nina Balthasar,[4] Roberto Coppari,[4] Heike Münzberg,[5] Marya Shanabrough,[6] Denis Burdakov,[7] Eva Rother,[1] Ruth Janoschek,[1] Jens Alber,[1] Bengt F. Belgardt,[1] Linda Koch,[1] Jost Seibler,[8,9] Frieder Schwenk,[8,9] Csaba Fekete,[10] Akira Suzuki,[11] Tak W. Mak,[12] Wilhelm Krone,[2] Tamas L. Horvath,[6] Frances M. Ashcroft,[3] and Jens C. Brüning[1]

[1]Department of Mouse Genetics and Metabolism, Institute for Genetics, University of Cologne and Center of Molecular Medicine Cologne (CMMC), Cologne, Germany. [2]Klinik II und Poliklinik für Innere Medizin, University of Cologne and CMMC, Cologne, Germany. [3]University Laboratory of Physiology, University of Oxford, Oxford, United Kingdom. [4]Department of Medicine, Division of Endocrinology, Beth Israel Deaconess Medical Center and Harvard Medical School, Boston, Massachusetts, USA. [5]Division of Metabolism, Endocrinology, and Diabetes, Department of Internal Medicine, and Department of Molecular and Integrative Physiology, University of Michigan Medical School, Ann Arbor, Michigan, USA. [6]Department of Obstetrics, Gynecology, and Reproductive Sciences and Department of Neurobiology, Yale University School of Medicine, New Haven, Connecticut, USA. [7]Faculty of Life Sciences, University of Manchester, Manchester, United Kingdom. [8]Artemis Pharmaceuticals, Cologne, Germany. [9]Fachhochschule Gelsenkirchen, Fachbereich Angewandte Naturwissenschaften, Gelsenkirchen, Germany. [10]Laboratory of Endocrine Neurobiology, Institute of Experimental Medicine, Hungarian Academy of Sciences, Budapest, Hungary. [11]Department of Molecular Biology, Akita University School of Medicine, Akita, Japan. [12]Department of Medical Biophysics, and Advanced Medical Discovery Institute and The Campbell Family Institute for Breast Cancer Research, Ontario Cancer Institute, University of Toronto, Toronto, Ontario, Canada.

Leptin and insulin have been identified as fuel sensors acting in part through their hypothalamic receptors to inhibit food intake and stimulate energy expenditure. As their intracellular signaling converges at the PI3K pathway, we directly addressed the role of phosphatidylinositol$_{3,4,5}$-trisphosphate–mediated (PIP_3-mediated) signals in hypothalamic proopiomelanocortin (POMC) neurons by inactivating the gene for the PIP_3 phosphatase Pten specifically in this cell type. Here we show that POMC-specific disruption of Pten resulted in hyperphagia and sexually dimorphic diet-sensitive obesity. Although leptin potently stimulated Stat3 phosphorylation in POMC neurons of POMC cell–restricted Pten knockout (PPKO) mice, it failed to significantly inhibit food intake in vivo. POMC neurons of PPKO mice showed a marked hyperpolarization and a reduction in basal firing rate due to increased ATP-sensitive potassium (K_{ATP}) channel activity. Leptin was not able to elicit electrical activity in PPKO POMC neurons, but application of the PI3K inhibitor LY294002 and the K_{ATP} blocker tolbutamide restored electrical activity and leptin-evoked firing of POMC neurons in these mice. Moreover, icv administration of tolbutamide abolished hyperphagia in PPKO mice. These data indicate that PIP_3-mediated signals are critical regulators of the melanocortin system via modulation of K_{ATP} channels.

Introduction

Obesity and diabetes mellitus type 2 represent a steadily increasing health risk worldwide (1). Therefore, research on the mechanisms regulating energy homeostasis, i.e., the balance between food intake and energy expenditure, has rapidly expanded in recent years. The identification of leptin as a fuel sensor, secreted by adipose tissue and acting in part through its hypothalamic receptor to inhibit food intake and stimulate energy expenditure, has provided the prototype for homeostatic signals that integrate the energy state of peripheral organs and the action of the central nervous system (2). Furthermore, the pancreas-derived peptide hormone insulin is secreted both short term, in response to rising blood glucose concentrations, and long term, in relation to fat mass (3–5). In addition to their expression in classical insulin target tissues such as liver, skeletal muscle, and adipose tissue, insulin receptors are widely distributed throughout the central nervous system, and insulin has been demonstrated to cross the blood-brain barrier to act on these receptors (6, 7).

Injection of leptin and insulin icv results in acute inhibition of food intake and activation of the sympathetic nervous system (8). Leptin and insulin receptors are particularly highly expressed in the arcuate nucleus of the hypothalamus (ARC) (9, 10). Within the ARC, they are coexpressed in neurons expressing the appetite-suppressing (anorexigenic) neuropeptides proopiomelanocortin (POMC, the precursor of α melanocyte-stimulating hormone [α-MSH]) and cocaine- and amphetamine-regulated transcript (CART) and in neurons expressing the appetite-inducing (orexigenic) neuropeptide Y (NPY) and agouti-related peptide (AgRP) (11–13). Thus, major sites for insulin and leptin action in the central nervous system appear to be NPY/AgRP- and POMC/CART-expressing neurons of the ARC (14–16). Toxin-mediated ablation of these cells has recently demonstrated that they play a

Nonstandard abbreviations used: aCSF, artificial cerebrospinal fluid; AgRP, agouti-related peptide; ARC, arcuate nucleus of the hypothalamus; CO_{Arte1}, *PomcCre-Pten$^{+/+}$-RosaArte1*; $CO_{Z/EG}$, *PomcCre-Pten$^{+/+}$-LacZ/EGFP*; IRS, insulin receptor substrate; HFD, high-fat diet; K_{ATP}, ATP-sensitive potassium; α-MSH, α melanocyte–stimulating hormone; ND, normal chow diet; NPY, neuropeptide Y; p-, phosphorylated; PB, phosphate buffer; PIP_3, phosphatidylinositol$_{3,4,5}$-trisphosphate; POMC, proopiomelanocortin; PPKO, POMC cell–restricted Pten knockout; $PPKO_{Arte1}$, *PomcCre-Pten$^{lox/lox}$-RosaArte1*; $PPKO_{Z/EG}$, *PomcCre-Pten$^{lox/lox}$-LacZ/EGFP*; PVN, paraventricular hypothalamic nucleus.

Conflict of interest: The authors have declared that no conflict of interest exists.

Citation for this article: *J. Clin. Invest.* **116**:1886–1901. doi:10.1172/JCI27123.

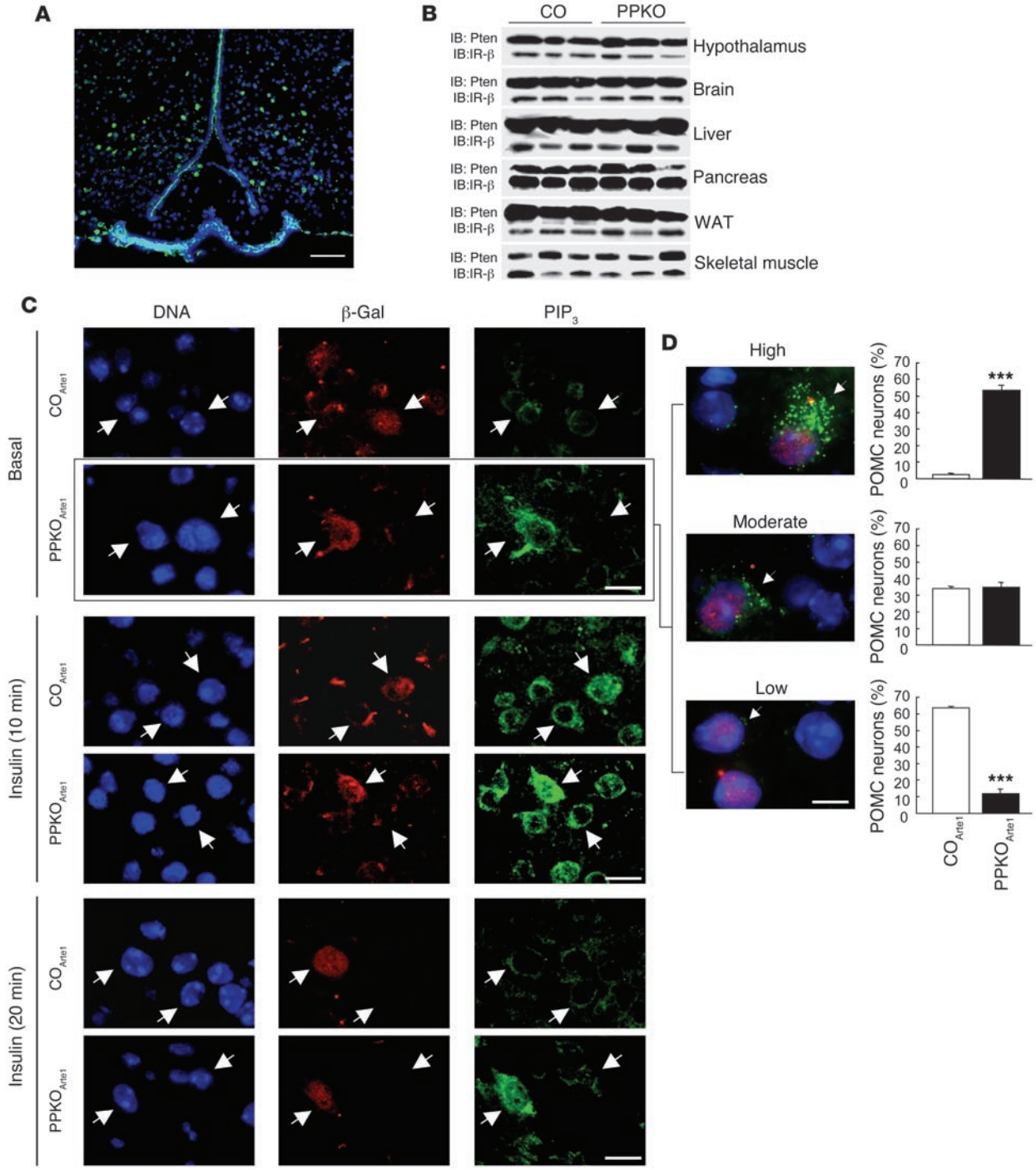

Figure 1

Generation of PPKO and reporter mice. (**A**) To visualize Cre-mediated recombination, immunohistochemistry for β-gal was performed in hypothalamic tissues of double-heterozygous reporter mice (*PomcCre-RosaArte1*). Blue (DAPI), DNA; green, β-gal. (**B**) Western blot analysis of Pten and insulin receptor β (IR-β) subunit in hypothalamus, brain, liver, pancreas, white adipose tissue (WAT), and skeletal muscle of control (CO) and PPKO mice. (**C**) PIP_3 formation in hypothalamic neurons of control and PPKO mice. Double immunohistochemistry of ARC neurons of CO_{Arte1} and $PPKO_{Arte1}$ reporter mice was performed in mice fasted overnight, which were injected intravenously with either saline or insulin and sacrificed 10 and 20 minutes after insulin stimulation. Arrows indicate 1 POMC and 1 non-POMC neuron in each panel. (**D**) Quantification of PIP_3 levels in control and PPKO POMC neurons in the basal (fasted) state. Values are mean ± SEM of sections obtained from 3 control and 3 PPKO mice. A total of 808 POMC neurons were analyzed. At left are examples of different magnitudes of PIP_3 immunoreactivity (arrowheads) as described in Methods. Blue (DAPI), DNA; red, β-gal (POMC neurons); green, PIP_3. ***$P \leq 0.001$ versus control. Scale bars: 100 μm (**A**), 20 μm (**C**), 10 μm (**D**).

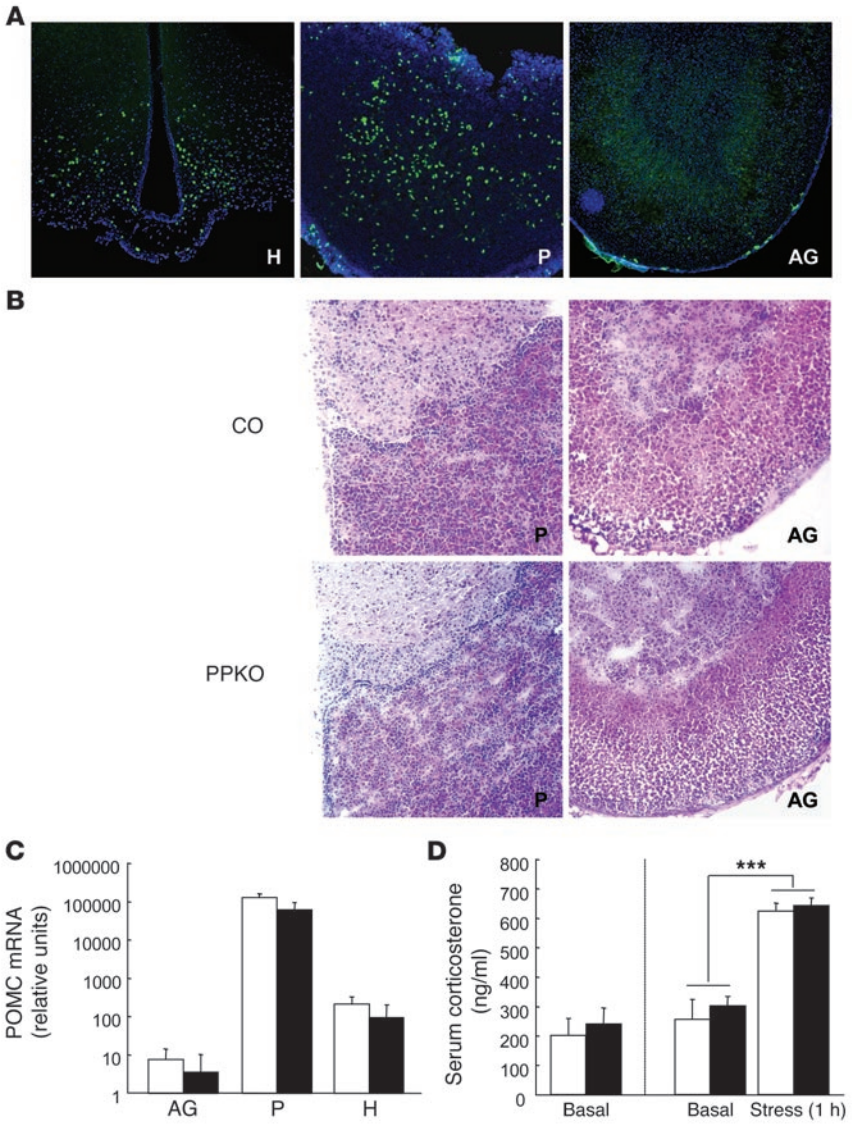

Figure 2
Unaltered regulation of the hypothalamo-pituitary-adrenal axis in PPKO mice. (**A**) Cre-mediated β-gal expression in a double-heterozygous reporter mouse (*PomcCre-RosaArte1*) in the ARC of the hypothalamus (H) and the anterior pituitary (P). No β-gal expression was observed in the adrenal gland (AG). (**B**) Representative H&E stain of the pituitary and the adrenal gland of a male control and a male PPKO mouse at the age of 12 weeks showed unaltered histomorphology of these organs in PPKO mice. (**C**) POMC mRNA expression in pituitary, hypothalamus, and adrenal gland of PPKO (black bars) and control (white bars) females on HFD at 12 weeks of age showed unaltered pituitary POMC expression in PPKO mice. Values are mean ± SEM (n = 6 per genotype). (**D**) Basal serum corticosterone levels at 12 weeks in PPKO (black bars) and control (white bars) HFD-fed females (left panel). Basal and stress-induced serum corticosterone levels at 12 weeks in PPKO and control SD males (right panel). Values are mean ± SEM (n = 6 per genotype). ***$P \leq 0.001$ versus basal. Magnification, ×100.

pivotal role in the acute regulation of feeding in adult mammals (17). Furthermore, icv injection of insulin and leptin results in reduced expression of NPY and AgRP and increased expression of POMC (18, 19). α-MSH stimulates melanocortin 4 receptors (MC4Rs) in target cells (which in turn activates the melanocortin signaling pathway), and coadministration of a MC4R-blocking agent prevents the ability of both insulin and leptin to inhibit food intake acutely. This provides further evidence that the melanocortin pathway plays an essential role in the action of both insulin and leptin (11, 20).

Leptin receptors belong to the family of cytokine receptors that acts via the Jak/Stat signaling pathway to regulate POMC expression in neurons (21). Insulin receptors are membrane-bound tyrosine kinases and do not stimulate the Jak/Stat pathway. However, both receptors efficiently activate insulin receptor substrate (IRS) protein–dependent signaling pathways by phosphorylating IRS proteins on tyrosine residues, either via the Jak2-dependent pathway (in case of leptin) or directly through the insulin receptor (in case of insulin, ref. 22). One of the major downstream pathways activated by IRS proteins involves recruitment of the regulatory subunit of PI3K to tyrosine-phosphorylated IRS proteins, leading to subsequent activation of the lipid kinase and the phosphorylation of phosphatidylinositol$_{4,5}$-bisphosphate to phosphatidylinositol$_{3,4,5}$-trisphosphate (PIP_3) (23). Therefore, activation of the PI3K pathway represents a point of convergence between insulin and leptin signaling. In accordance with this idea, icv injection of PI3K inhibitors partly abolishes the ability of both insulin and leptin to inhibit food intake (24, 25). Interestingly, however, while both insulin and leptin have been shown to activate PI3K in POMC neurons, they regulate PI3K in AgRP neurons differentially (26).

To directly address the role of PIP_3-dependent signaling in POMC-expressing neurons with respect to energy homeostasis in vivo, we inactivated the PIP_3 phosphatase Pten specifically in this cell type by Cre/loxP–mediated recombination. This is expected to promote continuous activation of the PI3K pathway. We then analyzed these mice with respect to their energy homeostasis.

Surprisingly, POMC cell–restricted Pten knockout (PPKO) mice exhibited hyperphagia and developed an obese phenotype. This was accompanied by resistance to leptin action in vivo despite unaltered leptin-stimulated Stat3 phosphorylation in POMC neurons. POMC neurons of PPKO mice were hyperpolarized and electrically silenced due to an increase in ATP-sensitive potassium (K_{ATP}) conductance. Inhibition of both PI3K activity and K_{ATP} channels restored electrical activity of PPKO POMC neurons. Importantly, blocking K_{ATP} channels selectively in the central nervous system by icv application of tolbutamide reversed hyperphagia in PPKO mice in vivo, assigning PI3K-dependent regulation of K_{ATP} channels in POMC neurons a central role in the regulation of energy homeostasis.

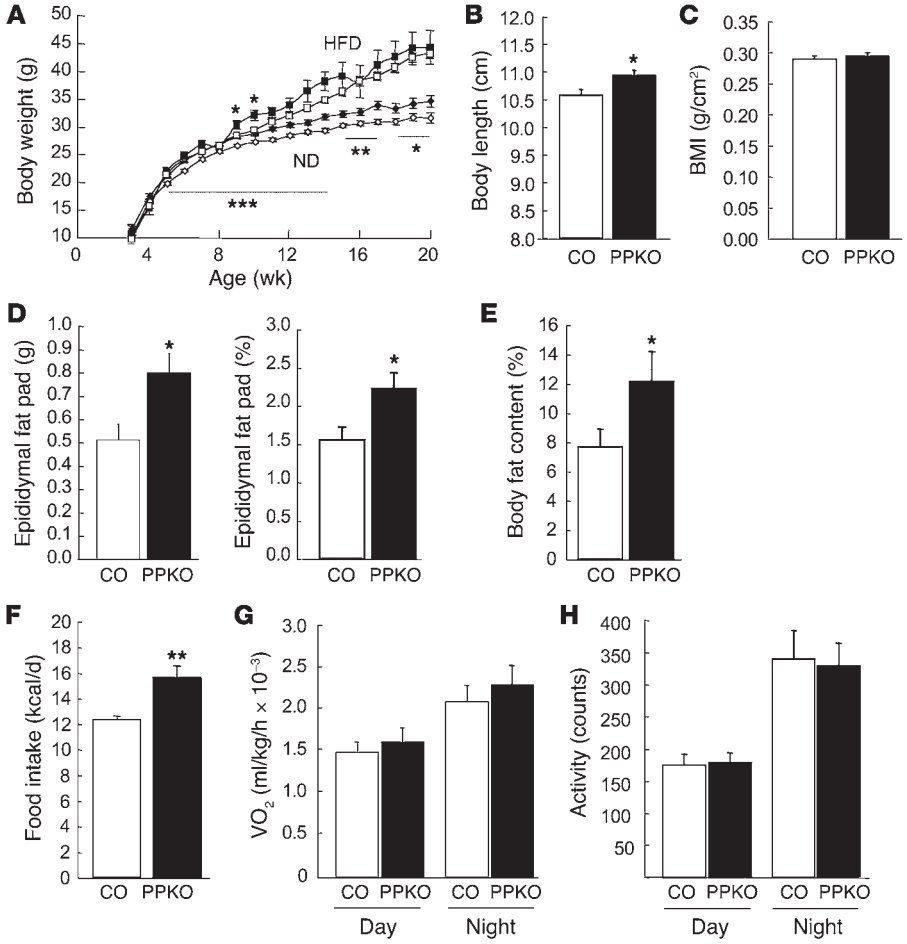

Figure 3
Phenotypic characteristics of control (open symbols; white bars) and PPKO (filled symbols; black bars) male mice under different dietary conditions with respect to energy homeostasis. (**A**) Average body weights of male mice on ND (diamonds) or HFD (squares) (n = 4–93). (**B**) Average body length of males on ND (n = 13–22). (**C**) BMI of male ND-fed control and PPKO mice (n = 13–22). (**D**) Absolute and relative (corrected for body weight) epididymal fat pad weights of ND-fed control and PPKO males (n = 15–22). (**E**) Body fat content of male ND-fed PPKO and control males as measured by dual-energy X-ray absorptiometry (n = 10–16). (**F**) Daily caloric intake of ND-fed control and PPKO males at the age of 10–13 weeks (n = 6 per genotype). (**G**) Oxygen consumption (VO_2) of male body weight–matched ND-fed mice at the age of 12 weeks (n = 4 per genotype). (**H**) Locomotor activity of body weight–matched ND-fed males at the age of 12 weeks (n = 4 per genotype). Unless otherwise indicated, data were collected at 20 weeks of age. Values are mean ± SEM. $^*P \le 0.05$, $^{**}P \le 0.01$, $^{***}P \le 0.001$ versus control.

Results

Generation of PPKO mice. Mice carrying the loxP-flanked (floxed) *Pten* allele (27) were crossed with mice expressing the *Cre* recombinase under control of the *Pomc* promoter (14). Cre-mediated recombination was visualized with the aid of a reporter mouse strain in which transcription of a β-*gal* gene under control of the ubiquitously expressed *Rosa26* promoter is prevented by a floxed hygromycin resistance gene (*RosaArte1*). Expression of β-gal in *PomcCre-RosaArte1* mice resembled the expression pattern described for POMC in the ARC (Figure 1A), i.e., inactivation of Pten was restricted to POMC neurons. Consistently, Western blot analysis revealed no changes in the overall expression of the Pten protein in brain and hypothalamus (Figure 1B). Moreover, Pten expression in peripheral tissues remained unaltered in PPKO mice (Figure 1B). Consistent with the expression pattern of endogenous POMC, peripheral Cre-mediated recombination was detectable in the pituitary but not in the adrenal gland (Figure 2A). However, both young and old PPKO mice exhibited normal pituitary and adrenal histomorphology (Figure 2B). Moreover, POMC mRNA levels were unaltered in these organs (Figure 2C). Functionally, both basal and stress-induced serum corticosterone levels were unchanged in PPKO mice (Figure 2D). This excludes the possibility that Pten deficiency in POMC-expressing cells of the pituitary causes impaired corticosterone regulation.

We next determined the functional effects of POMC neuron–restricted Pten deficiency on PIP_3 formation in control *PomcCre-Pten*$^{+/+}$-*RosaArte1* (CO_{Arte1}) and *PomcCre-Pten*$^{lox/lox}$-*RosaArte1* ($PPKO_{Arte1}$) reporter mice, which both express β-gal in POMC neurons. In the basal state, little immunoreactive PIP_3 was detectable in POMC and adjacent neurons of control reporter mice. POMC neurons of $PPKO_{Arte1}$ mice exhibited high levels of immunodetectable PIP_3, while adjacent neurons exhibited immunoreactive PIP_3 at levels comparable to ARC neurons of control mice (Figure 1C, top 2 rows). Quantitative analysis of basal PIP_3 levels in POMC neurons showed a significantly higher percentage of POMC neurons with vastly increased PIP_3 levels in $PPKO_{Arte1}$ compared with control mice. Strikingly, only 12% of $PPKO_{Arte1}$ POMC neurons — as opposed to 64% of control POMC neurons — exhibited very little or no PIP_3 (Figure 1D). After stimulation with insulin for 10 minutes, high levels of immunoreactive PIP_3 were detectable in virtually all hypothalamic neurons with the highest levels in POMC cells of $PPKO_{Arte1}$ mice (Figure 1C, middle 2 rows). In CO_{Arte1} mice and non-POMC neurons of $PPKO_{Arte1}$, PIP_3 levels decreased to levels comparable to the basal state within 20 minutes after insulin stimulation, but POMC neurons of $PPKO_{Arte1}$ mice still displayed high levels of immunodetectable PIP_3 (Figure 1C, bottom 2 rows).

Diet-sensitive obesity in PPKO mice is gender dimorphic. Analysis of the physiological impact of PIP_3 elevation specifically in POMC neurons of PPKO mice revealed a significant and stable increase in the body weight of PPKO males on a normal chow diet (ND) compared with controls (Figure 3A). The body weight of PPKO males fed a high-fat diet (HFD) was initially slightly higher than

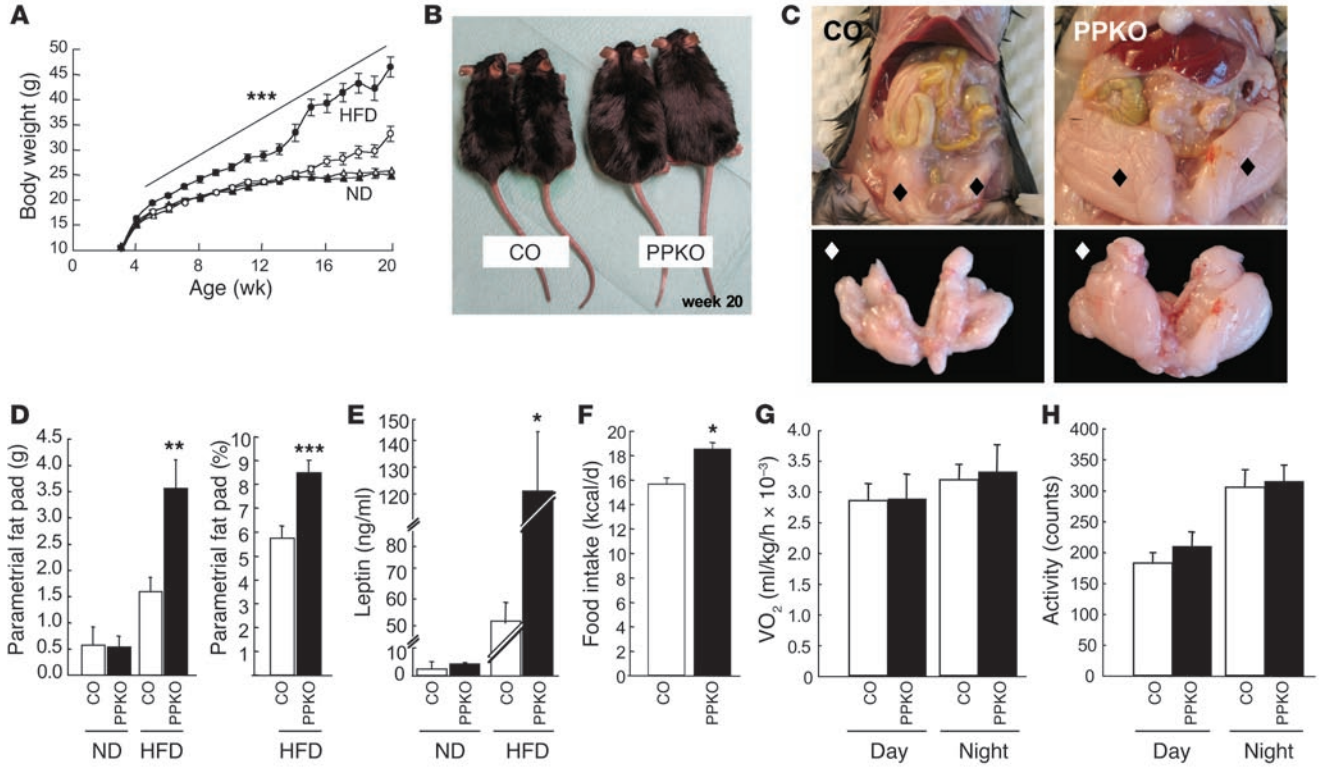

Figure 4

Phenotypic characteristics of control (open symbols; white bars) and PPKO (filled symbols; black bars) female mice under different dietary conditions with respect to energy homeostasis. (**A**) Average body weight of ND- (triangles) and HFD-fed (circles) female mice (n = 6–81). (**B**) Outward appearance of 2 control and 2 PPKO female mice of the same litter at the age of 20 weeks (17 weeks of HFD feeding). (**C**) Exemplary demonstration of parametrial fat pads in situ (upper panel; black diamonds) and ex situ (lower panel; white diamonds) of control and PPKO females at the age of 20 weeks. (**D**) Absolute parametrial fat pad weights of female control and PPKO mice on ND and HFD (n = 3–17) and relative (corrected for body weight) parametrial fat pad weights of female HFD-fed control and PPKO mice. (**E**) Serum leptin levels of female control and PPKO mice on ND and HFD (n = 4–30). (**F**) Daily caloric intake of female control and PPKO mice on HFD at the age of 10–13 weeks (n = 4–6). (**G**) Oxygen consumption of female mice on HFD at the age of 12 weeks (n = 7–8). (**H**) Locomotor activity of female mice on HFD at the age of 12 weeks (n = 7–8). Unless otherwise indicated, data were collected at 20 weeks of age. Values are mean ± SEM. $^*P \leq 0.05$, $^{**}P \leq 0.01$, $^{***}P \leq 0.001$ versus control.

that of the respective controls but became indistinguishable by the age of 15 weeks (Figure 3A). Consistent with the growth curves, at 20 weeks, ND-fed PPKO males displayed significantly increased absolute and relative (corrected for body weight) epididymal fat pad weights compared with controls (Figure 3D). Determination of body composition using direct digital densitometry demonstrated a significantly higher (60% increase) mean body fat content in ND-fed PPKO males (Figure 3E), indicating that the amount of epigonadal fat pads represents an adequate indicator of total body fat in these mice. In addition to the increased body weight, PPKO mice showed significantly increased body length at the age of 20 weeks (Figure 3B). Consequently, BMI was comparable for male ND-fed PPKO and control mice (Figure 3C) and thus fails to serve as an indicator of adiposity in this model.

In female mice, body weight did not differ on ND, but HFD-fed PPKOs exhibited significantly elevated body weights, gaining 40% more body weight than controls by the age of 20 weeks (Figure 4, A and B). The obesity of PPKO females on HFD was characterized by early onset and increased continuously over time without reaching a plateau or set point. Like ND-fed PPKO males, female PPKOs on HFD displayed a significant 2-fold increase in absolute and relative epigonadal fat pad weights compared with their respective control littermates (Figure 4, C and D). The increased obesity of PPKO females on HFD was also reflected in a marked increase in circulating plasma leptin concentrations (Figure 4E).

Hyperphagia in PPKO mice. To gain further insights into the mechanisms resulting in obesity in PPKO mice, we measured energy intake and expenditure in vivo. Food intake was significantly greater in both ND-fed PPKO males and HFD-fed PPKO females compared with control mice (Figure 3F and Figure 4F). In contrast, oxygen consumption (Figure 3G and Figure 4G), locomotor activity (Figure 3H and Figure 4H), and respiratory exchange ratio and body core temperature (data not shown) of PPKO mice were indistinguishable from controls. Thus, obesity in PPKO mice results from hyperphagia in the absence of altered energy expenditure.

Increased perikaryal size and efferent projections of POMC cells in PPKO mice. The hyperphagia-induced obesity and increased body length of PPKO mice suggests that the melanocortin pathway may be impaired by Pten inactivation in POMC neurons. Thus, we next determined whether the number, survival, or projection of POMC cells was altered. Quantitative assessment of β-gal–expressing POMC neurons in control and PPKO mice revealed no changes in the number

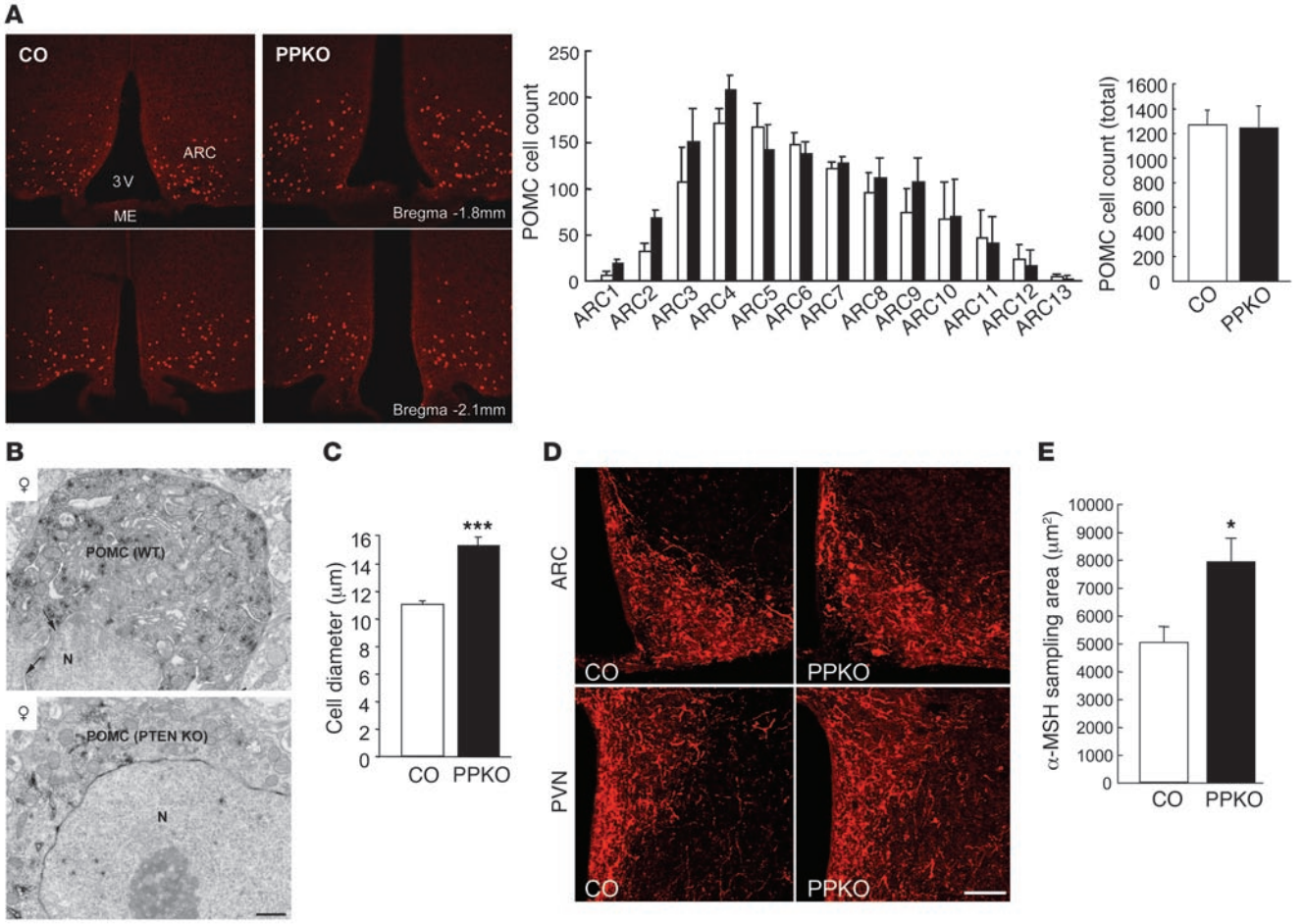

Figure 5

Number, morphology, and projecting fibers of POMC neurons in control (white bars) and PPKO (black bars) mice. (**A**) Left: Immunohistochemical visualization of Cre-mediated β-gal expression in 12-week-old ND-fed male CO_{Arte1} and $PPKO_{Arte1}$ reporter mice in the ARC. ME, median eminence; 3V, third ventricle. POMC cell counts in different regions of the ARC (center) and in the total ARC tissue (right) showed an unaltered number of POMC cells in PPKO mice (n = 3–4). (**B**) Ultrastructural characteristics of POMC neurons in female HFD-fed control and PPKO mice at the age of 11 weeks. N, nucleus. (**C**) Quantification of the POMC cell size in hypothalamic tissues of female HFD-fed control and PPKO mice at the age of 11 weeks (n = 26–28 POMC cells from 3 independent mice per genotype). (**D**) α-MSH staining of hypothalamic projecting fibers in the ARC and PVN of 20 week-old control and PPKO females on HFD. (**E**) Quantification of α-MSH content in projections of control and PPKO POMC neurons in 20 week-old control and PPKO females on HFD (n = 13–20 measurements from 4 control and 5 PPKO mice). Values are mean ± SEM. *$P \leq 0.05$; ***$P \leq 0.001$ versus control. Scale bars: 1 μm (**B**), 100 μm (**D**). Magnification, ×100 (**A**).

or distribution of POMC cells within different regions of the ARC (Figure 5A). In addition, there were no apparent signs of damaged intracellular organelles in POMC neurons of PPKO mice as revealed by electron microscopy. However, the average diameter of POMC perikarya was significantly higher in PPKO animals compared with wild-type littermates (Figure 5B). Quantitative assessment of POMC cell size by measuring soma size after immunostaining for endogenous α-MSH revealed a significant increase in POMC cell diameter of PPKO mice (Figure 5C). In line with the increased soma size of POMC neurons, α-MSH–immunolabeled efferents were more abundant in the ARC and paraventricular hypothalamic nucleus (PVN) of PPKO mice compared with their wild-type littermates (Figure 5, D and E). Thus, while Pten deficiency does not appear to affect differentiation and proliferation of POMC cells, it promotes efferent outgrowth of these neurons resulting in a more robust innervation of target areas by melanocortin efferents.

Leptin resistance but normal neuropeptide expression in PPKO mice. We next used quantitative RT-PCR to analyze the expression of anorexigenic (POMC/α-MSH, CART) and orexigenic (AgRP, NPY) neuropeptides. We also examined expression of thyrotropin-releasing hormone (TRH) and corticotropin-releasing hormone (CRH), potential targets of α-MSH action in second-order neurons of the PVN. Around the onset of obesity at 6 weeks of age, POMC expression was increased 3.5-fold in female HFD-fed PPKOs compared with controls, indicating that early obesity developed despite significantly increased POMC expression (Figure 6A). Notably, despite the marked increase in POMC mRNA, neither TRH nor CRH mRNAs were increased. This suggests that α-MSH release or action is impaired. At 20 weeks (i.e., after the onset of obesity), NPY expression was significantly reduced in PPKO females (Figure 6A).

We next determined leptin sensitivity in 15-week-old ND-fed male control and PPKO mice, which showed indistinguishable

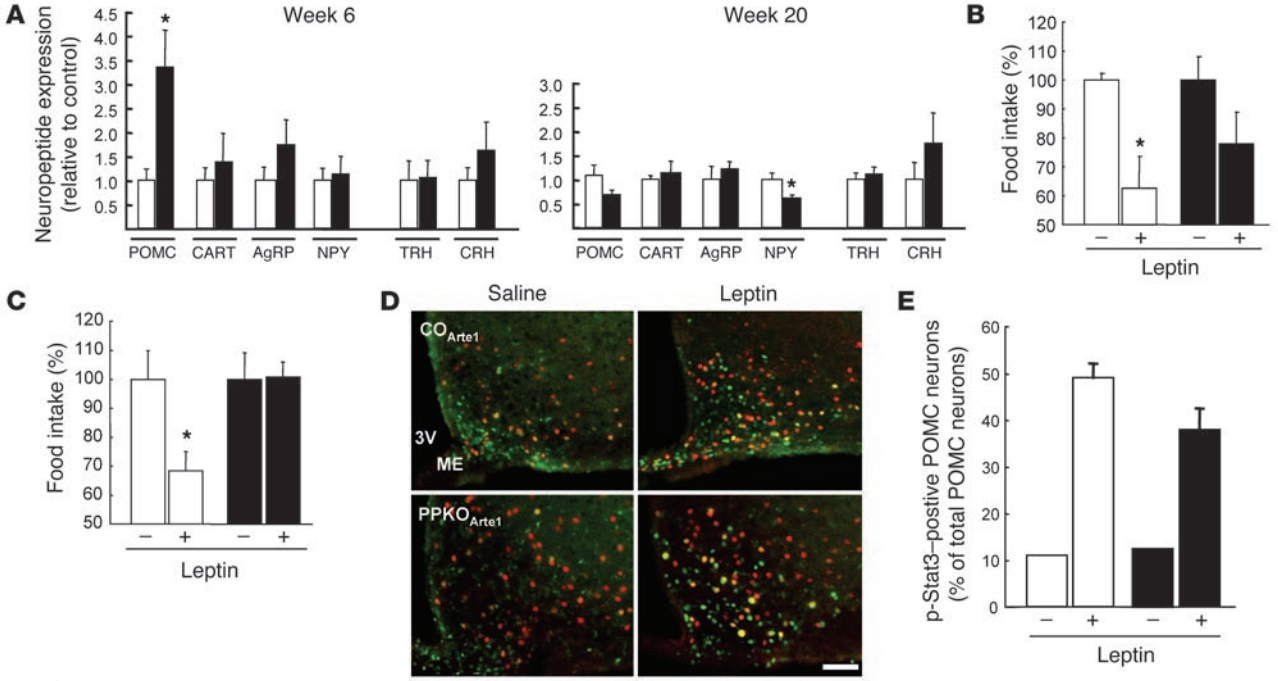

Figure 6

Hypothalamic neuropeptide expression and assessment of leptin sensitivity in control (white bars) and PPKO (black bars) mice. (**A**) Neuropeptide expression HFD-fed female mice at 6 and 20 weeks of age (n = 7–9 per group). CART, cocaine- and amphetamine-regulated transcript; AgRP, agouti-related peptide; TRH, thyrotropin-releasing hormone; CRH, corticotropin-releasing hormone. (**B** and **C**) Changes in food intake after intraperitoneal leptin treatment in ND-fed males at 15 weeks of age (**B**) and HFD-fed females at 10 weeks of age (**C**). Data represent daily food intake after a 3-day treatment with twice-daily injections of saline (–) or 2 mg/kg leptin (+; n = 4–6 per group). (**D**) Representative immunohistochemistry of pStat3 formation in hypothalamic neurons of male ND-fed control and PPKO mice at 12–15 weeks of age. Double immunohistochemistry of ARC neurons of CO_{Arte1} and $PPKO_{Arte1}$ reporter mice was performed in ad libitum–fed mice, which were intravenously injected with either saline or leptin and sacrificed 30 minutes after the injection. Red, β-gal (POMC neurons); green, pStat3. Scale bar: 100 μm. (**E**) Quantification of pStat3-positive POMC neurons in hypothalamic slices of male CO_{Arte1} and $PPKO_{Arte1}$ reporter mice on ND at the age of 12–15 weeks before (n = 1) and after (n = 3–8) leptin application ($P > 0.05$). Values are mean ± SEM. *$P \leq 0.05$.

serum leptin levels (control, 2.72 ± 0.66 ng/ml; PPKO, 2.1 ± 0.36 ng/ml; $P > 0.05$). Leptin treatment caused a 40% reduction in food intake in control mice but failed to produce a significant effect in PPKOs (Figure 6B). Similarly, leptin treatment of 10-week-old HFD-fed control and PPKO females, which both exhibited hyperleptinemic but similar serum leptin levels (control, 6.61 ± 0.58 ng/ml; PPKO, 8.52 ± 2.26 ng/ml; $P > 0.05$), resulted in a significant, 30% reduction of food intake in controls but had no detectable effect in PPKO mice (Figure 6C). Although hyperphagia as present in these mice has been demonstrated to result in leptin resistance (28), and it appears therefore difficult to separate the causative role of hyperphagia from POMC-restricted Pten deficiency, these data indicate that PPKO mice are leptin resistant in vivo. Under the same experimental conditions, leptin potently stimulated Stat3 phosphorylation in ARC neurons of male control and $PPKO_{Arte1}$ mice on ND both in POMC and in non-POMC neurons (Figure 6D). However, the percentage of POMC neurons with robust Stat3 phosphorylation after leptin administration tended to be slightly lower in PPKO than in control mice (Figure 6E). Nevertheless, leptin evoked a clear 3-fold stimulation of Stat3 phosphorylation in POMC cells of PPKO mice (Figure 6E). Taken together, these data indicate that POMC-restricted inactivation of the *Pten* gene results in augmentation of PIP_3 generation in POMC neurons but leads to diet-sensitive obesity and leptin resistance. The latter effect is mediated by a mechanism that appears, at least in part, to be independent of Stat3 phosphorylation and POMC transcription.

Increased ATP-sensitive potassium conductance in PPKO POMC neurons. Activation of the PI3K pathway has been linked to the regulation of K_{ATP} channels by insulin and leptin (29–32). K_{ATP} channels have been extensively characterized in peripheral tissues, where they link membrane excitability with the metabolic status of the cell (33). Opening of K_{ATP} channels leads to membrane hyperpolarization and diminished electrical activity. This suggests that inactivation of Pten may alter the excitability of PPKO POMC neurons. Interestingly, identified POMC neurons possess K_{ATP} currents and

Table 1

Electrical properties of POMC neurons in male and female PPKO mice

Parameters	Size (pF)	Vm (mV)	Firing (Hz)	Gm (pS/pF)
Male PPKO	27 ± 3	–51 ± 2	0.14 ± 0.06	105 ± 12
Female PPKO	39 ± 5	–53 ± 1	0.10 ± 0.07	97 ± 15

Values are mean data obtained from recordings from neurons identified by EGFP fluorescence (n = 10–11). $P > 0.05$ between male and female PPKO mice for all parameters. Gm, membrane conductance; Vm, resting membrane potential.

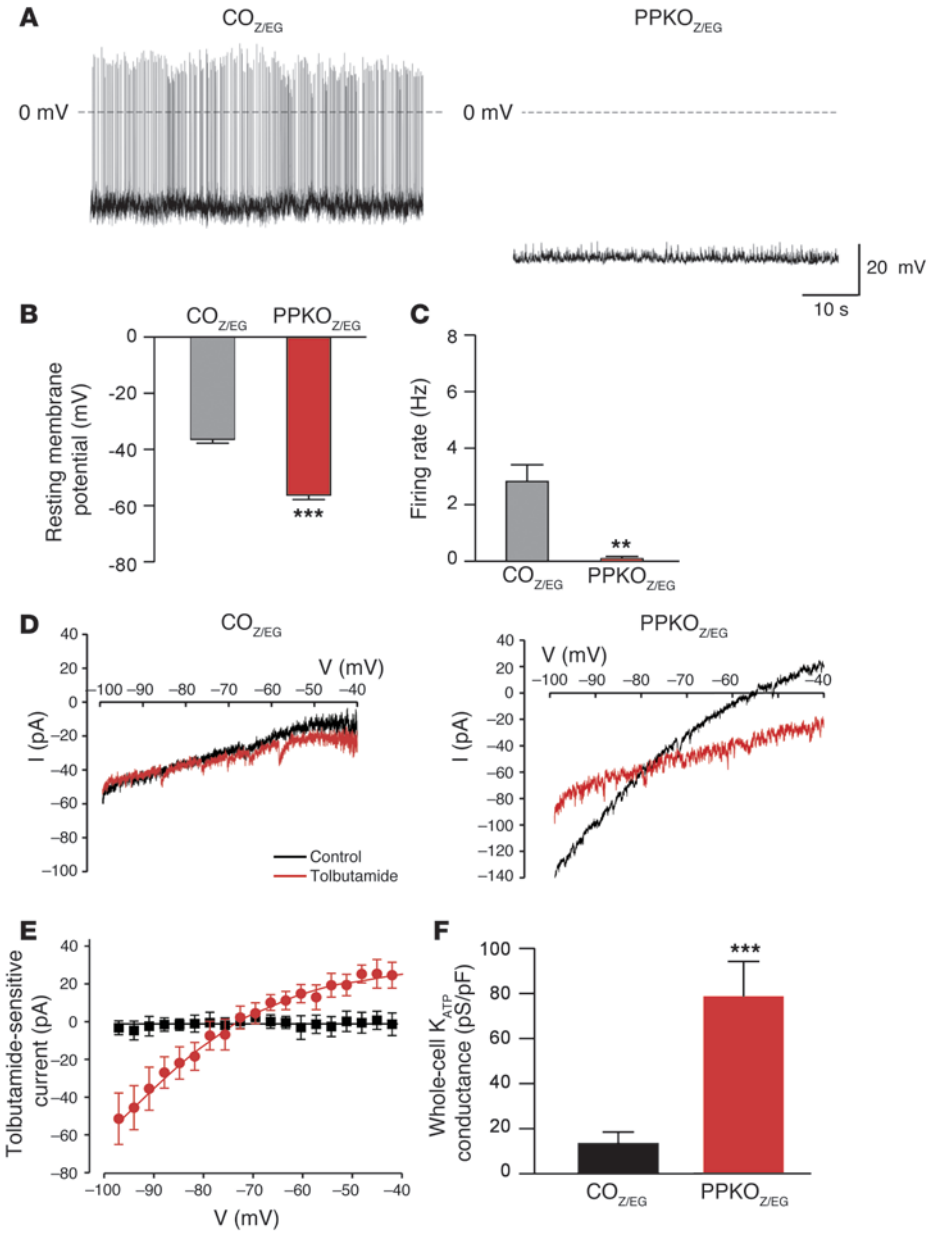

Figure 7
Genetic deletion of Pten increases K_{ATP} currents and silences POMC neurons. (**A**) Representative membrane potential recordings from identified POMC neurons in ARC slices from $CO_{Z/EG}$ and $PPKO_{Z/EG}$ mice. Note the absence of action potentials in $PPKO_{Z/EG}$ neurons. (**B**) Mean resting membrane potential of $CO_{Z/EG}$ and $PPKO_{Z/EG}$ POMC neurons (n = 10–12). (**C**) Mean action potential frequency of $CO_{Z/EG}$ and $PPKO_{Z/EG}$ POMC neurons (n = 10–12). (**D**) Current responses to voltage ramps from –100 to –40 mV (rate, 70 mV/s) in the absence (black) and presence (red) of 200 μM tolbutamide for the same $CO_{Z/EG}$ and $PPKO_{Z/EG}$ neurons as in **A**. Holding potential, –60 mV. I, electric current. (**E**) Mean tolbutamide-sensitive current-voltage relation for 4 $CO_{Z/EG}$ (black) and 6 $PPKO_{Z/EG}$ (red) neurons. Currents were normalized to cell capacitance to correct for differences in cell size, as $PPKO_{Z/EG}$ neurons (23 ± 5 pF; n = 10) were consistently larger than $CO_{Z/EG}$ neurons (9 ± 1 pF; n = 26). (**F**) Mean tolbutamide-sensitive conductance for $CO_{Z/EG}$ and $PPKO_{Z/EG}$ POMC neurons. Conductance was measured as the slope of the tolbutamide-sensitive current-voltage relation between –70 mV and –95 mV. Conductances were normalized to cell capacitance. Same neurons as in **E**. Values are mean ± SEM. $^{**}P \leq 0.01$, $^{***}P \leq 0.001$ versus $CO_{Z/EG}$.

express the K_{ATP} channel subunits Kir6.2 and SUR1 (34). Although glucose stimulates (34) and insulin inhibits (35) the electrical activity of POMC neurons, it has not been directly demonstrated that they do so by acting on K_{ATP} channels. Leptin also increases electrical activity of POMC neurons, but it has been suggested to act via a different mechanism to insulin (36).

To test the impact of the POMC neuron–specific disruption of Pten on K_{ATP} channel activation and neuronal excitability, mice were generated in a second reporter cross with the *LacZ/EGFP* (*Z/EG*) strain (37). By analogy with the *Arte1* reporter mice, the 2 groups, which both express EGFP in POMC neurons due to Cre-mediated recombination, are referred to as $CO_{Z/EG}$ (*PomcCre-Pten*$^{+/+}$-*LacZ/EGFP*) and $PPKO_{Z/EG}$ (*PomcCre-Pten*$^{lox/lox}$-*LacZ/EGFP*) mice.

Electrical activity of identified POMC neurons in the ARC of both male and female mice was substantially lower, and the membrane potential was more hyperpolarized in $PPKO_{Z/EG}$ than in $CO_{Z/EG}$ mice (Tables 1 and 2 and Figure 7, A–C). In total, 12 out of 16 $PPKO_{Z/EG}$ neurons were electrically silent. Addition of the K_{ATP} channel blocker tolbutamide increased the mean firing frequency of $PPKO_{Z/EG}$ neurons more than $CO_{Z/EG}$ neurons (270-fold and 2-fold, respectively), suggesting K_{ATP} channel activity makes a greater contribution to the membrane conductance of $PPKO_{Z/EG}$ neurons (Tables 2 and 3). To address this possibility, we quantified the K_{ATP} conductance by measuring the difference in membrane conductance in the presence and absence of tolbutamide (Figure 7D). The K_{ATP} conductance was 6.6-fold greater in $PPKO_{Z/EG}$ than in $CO_{Z/EG}$ neurons, whereas the tolbutamide-insensitive conductance was not significantly different (Figure 7, E and F). Thus activation of K_{ATP} channels strongly contributes to silencing of $PPKO_{Z/EG}$ neurons. The larger K_{ATP} conductance is consistent with the elevated levels of PIP_3 in $PPKO_{Z/EG}$ neurons and the fact that the lipid stimulates K_{ATP} channel activity and reduces its sensitivity to inhibition by ATP (38).

Table 2
Electrical properties of POMC neurons in control and PPKO mice

Parameters	$CO_{Z/EG}$ neurons	$PPKO_{Z/EG}$ neurons
Capacitance (pF)	9 ± 1	23 ± 5[A]
Resting potential (mV)	–36 ± 1	–56 ± 2[A]
Firing frequency (Hz)	3.3 ± 0.5	0.095 ± 0.089[A]
Membrane conductance (pS/pF)	111 ± 16	184 ± 24[B]
K_{ATP} conductance (pS/pF)	13 ± 5	86 ± 17[C]
Non-K_{ATP} conductance (pS/pF)	69 ± 9	64 ± 12

Values are mean ± SEM obtained from recordings from neurons identified by EGFP fluorescence. For $CO_{Z/EG}$, $n = 12$; for $PPKO_{Z/EG}$, $n = 10$; for K_{ATP} and non-K_{ATP} conductance values, $n = 5$. [A]$P \le 0.001$. [B]$P \le 0.05$. [C]$P \le 0.01$.

To further investigate whether the increased K_{ATP} conductance and reduced electrical activity of PPKO POMC neurons indeed arises from the increase in PIP_3, we tested the effect of the PI3K inhibitor LY294002. Inhibition of PIP_3 formation by LY294002 normalized both the amplitude of the K_{ATP} conductance and the firing rate of $PPKO_{Z/EG}$ neurons (Figure 8, A–C). However, LY294002 did not affect firing rate or K_{ATP} conductance of $CO_{Z/EG}$ POMC neurons (Figure 8, B and C). Taken together, our results demonstrate that genetic deletion of Pten results in elevation of PIP_3, which leads to enhanced K_{ATP} currents and electrical silencing of POMC neurons, and that acute inhibition of PI3K reverses this effect.

K_{ATP} channel inhibition restores leptin's ability to elicit firing of PPKO POMC neurons and reverses hyperphagia of PPKO mice in vivo. Because α-MSH secreted by POMC neurons is a potent anorexigenic hormone, electrical silencing could provide one explanation for the enhanced food intake and increased propensity to obesity observed in PPKO mice. Furthermore, the leptin resistance of PPKO mice might arise because the inward current elicited by leptin (36) is too small to counteract the greater K_{ATP} currents of PPKO POMC neurons. To test this idea, we examined the ability of leptin to stimulate firing of POMC neurons in $PPKO_{Z/EG}$ mice. Leptin induced a small depolarization of $PPKO_{Z/EG}$ POMC neurons, from –58 ± 3 mV to –54 ± 2 mV ($n = 6$; $P \le 0.01$), but this was not sufficient to elicit electrical activity (Figure 9, A and B). Strikingly, however, coadministration of leptin and tolbutamide led to a more pronounced depolarization, which resulted in a firing rate that was significantly higher than that evoked by tolbutamide alone (Figure 9B). These data indicate that reversal of the increased K_{ATP} current in $PPKO_{Z/EG}$ POMC neurons (by tolbutamide) restores leptin's ability to increase firing in these cells (36) and imply that the leptin resistance of PPKO POMC neurons is a consequence of K_{ATP} channel activation.

The ability of tolbutamide to stimulate electrical firing of $PPKO_{Z/EG}$ POMC neurons and to restore leptin sensitivity suggests that the drug may be able to reverse the hyperphagia and obesity of PPKO mice. To test this idea, we infused tolbutamide into the lateral ventricle of the brain in 12-week-old males on ND, thereby selectively blocking central K_{ATP} channels. While this treatment did not affect food intake or body weight in control mice, it significantly abolished hyperphagia in PPKO mice and concomitantly reduced body weight in these mice (Figure 9C). This indicates that K_{ATP} channel activation in the brain contributes to the hyperphagic and obese phenotype of PPKO mice.

Finally we confirmed that, as previously reported (35), insulin indeed hyperpolarized the membrane potential and inhibited electrical activity in POMC neurons of control mice (Figure 10, A–C). Importantly, we also demonstrated that leptin was unable to stimulate electrical activity of POMC neurons in the presence of insulin (Figure 10, A and B). This is consistent with the failure of leptin to enhance electrical activity in POMC neurons of PPKO mice. On the other hand, we found that the K_{ATP} channel blocker tolbutamide restored leptin's ability to activate a control POMC neuron in the presence of insulin, again indicating that inactivation of POMC neurons by insulin occurs via K_{ATP} channel activation (Figure 10A).

Discussion

Activation of the PI3K signaling pathway in hypothalamic neurons provides a potential point of convergence for multiple hormones regulating energy homeostasis including leptin, insulin (22), NPY, and peptide YY (39). However, the exact role of this pathway in the regulation of food intake and energy expenditure has yet not been fully established. Because icv injection of PI3K inhibitors blocks the anorexigenic effects of both insulin and leptin (24, 25), it has been argued that PI3K signaling plays a key role in the actions of both hormones. However, the question of which particular ARC neurons are the primary targets for hormone-stimulated PI3K activation, and which of the downstream signaling events activated by PI3K are involved, has not been answered. Because insulin and leptin both directly target POMC neurons (16) and ablation of these neurons leads to impaired regulation of energy homeostasis (17), we reasoned that POMC neurons must be involved and that constitutive activation of PIP_3-dependent signaling in this cell type would be predicted to result in decreased food intake and increased leanness in mice.

Surprisingly, our results reveal that constitutive elevation of PIP_3 in POMC neurons in vivo resulted in gender-dimorphic, diet-sensitive obesity due to hyperphagia. This occurs in the presence of an increase in the K_{ATP} conductance of these neurons, which leads to membrane hyperpolarization and electrical silencing. Although the exact mechanism responsible for the sexual dimorphism of the phenotype is not clear, it is worth noting that insulin's anorectic effect also appears to be gender specific. Whereas icv injection of insulin acutely inhibits food intake in male rats, it fails to do so

Table 3
Mean data obtained from neurons in which tolbutamide was tested

	Before tolbutamide	After tolbutamide	Capacitance (pF)
$CO_{Z/EG}$ neurons			
Resting potential (mV)	–39 ± 3	–33 ± 3[A]	9.8 ± 1.0
Firing frequency (Hz)	3.2 ± 0.2	5.6 ± 0.6[A]	
Membrane conductance (pS/pF)	85 ± 18	69 ± 9[A]	
$PPKO_{Z/EG}$ neurons			
Resting potential (mV)	–58 ± 3	–49 ± 4[A]	30 ± 9
Firing frequency (Hz)	0.007 ± 0.006	1.86 ± 0.48[A]	
Membrane conductance (pS/pF)	157 ± 31	64 ± 12[A]	

Values are mean ± SEM (n = 5 per group). [A]$P \le 0.01$.

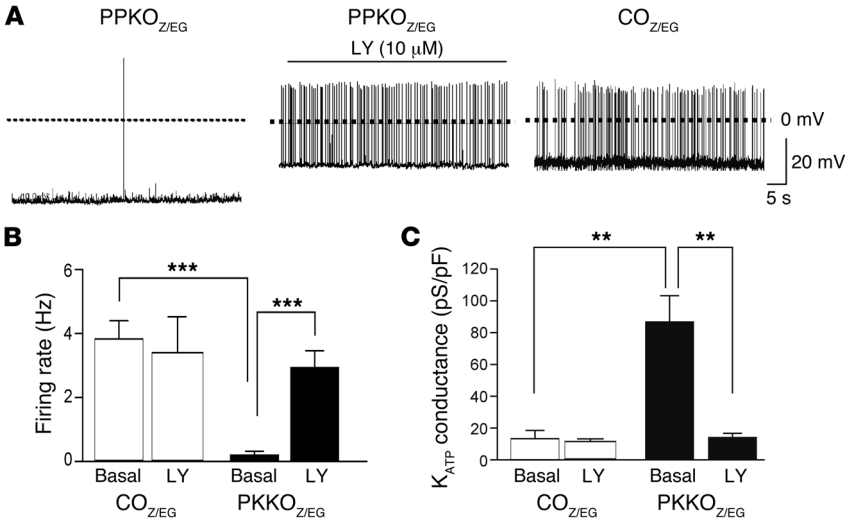

Figure 8
Effects of LY294002 (LY) on electrical activity of PPKO$_{Z/EG}$ POMC neurons. (**A**) Representative membrane potential recording from an identified POMC neuron in an ARC slice from a PPKO$_{Z/EG}$ mouse, before and after addition of 10 μM LY294002, compared with a representative membrane potential recording from an identified CO$_{Z/EG}$ POMC neuron. Mean action potential frequency (**B**) and mean K_{ATP} conductance (**C**) of PPKO$_{Z/EG}$ and CO$_{Z/EG}$ POMC neurons before and after addition of LY294002 to the medium (n = 8 per group). Values are mean ± SEM. *$P \leq 0.05$; **$P \leq 0.01$; ***$P \leq 0.001$.

in female rats (40), and genetic inactivation of the brain insulin receptor results in more pronounced weight gain in female mice than male mice (41). In females, neuronal insulin resistance due to insulin receptor deletion results in hypogonadism, thus offering a potential mechanism for the gender dimorphism. However, because reproductive function, as assessed by birth-to-birth interval and litter size, appeared to be intact in male and female PPKO mice (data not shown), overt hypogonadism is unlikely to account for the gender-specific effects we observed. Furthermore, the membrane hyperpolarization and reduced firing rates of PPKO POMC neurons were similar in male and female mice (Table 1). It therefore appears that Pten deletion may produce some different physiological effects dependent on gender. Although the underlying mechanism for this phenomenon is not clear at this point, our data are consistent with multiple knockout experiments targeting signaling pathways involved in the regulation of energy homeostasis that yielded as-yet unexplained gender-specific phenotypes (41–43). Thus, this is an area that clearly deserves further detailed analysis.

It has been previously demonstrated in vitro that PIP_3 activates K_{ATP} channels directly (44). Even though constitutive elevation of PIP_3 differs from the transient increase in PIP_3 produced by acute hormonal stimulation, our results now provide very strong evidence for the importance of this signaling pathway in hypothalamic neurons in vivo. In particular, the ability of icv tolbutamide to reverse the hyperphagia and obesity of PPKO mice emphasizes the central importance of K_{ATP} channels in determining the obese phenotype. Nevertheless, given the broad biological effects elicited by PI3K signaling, elevation of PIP_3 due to Pten inactivation may have effects in addition to activation of K_{ATP} channels. Indeed, both electron microscopy and measurements of cell capacitance revealed an increase in the size of POMC neurons in PPKO mice. This is consistent with previous reports that Pten controls cell size in *Drosophila* and murine neurons via regulation of S6 kinase activity (45, 46).

The marked increase in the K_{ATP} current of PPKO POMC neurons, together with the complete reversal of their electrophysiological phenotype upon pharmacological inhibition of PI3K activity, provides strong support for the idea that electrical silencing of POMC neurons results from PIP_3-mediated activation of K_{ATP} channels. Thus it is likely that a transient increase in PIP_3 formation upon hormonal stimulation will also lead to activation of K_{ATP} channels and subsequent silencing of POMC neurons. Consistent with this idea, insulin, which is a potent activator of PI3K, leads to K_{ATP} channel activation in unidentified hypothalamic neurons (31) and hyperpolarizes identified POMC neurons, thereby reducing their electrical activity (35) (Figure 10, A–C). Our experiments therefore suggest a molecular mechanism for how insulin hyperpolarizes POMC neurons — namely, K_{ATP} channel activation consequent on PIP_3 elevation (Figure 11). This model predicts that the anorexigenic effects of insulin are not mediated via POMC neurons, since mimicking insulin-induced activation of PI3K in POMC neurons of PPKO mice resulted in hyperphagia and obesity. Our data further suggest that although leptin enhanced PIP_3 in POMC neurons, and its effects are widely postulated to occur in part via PIP_3 activation, its main action in this cell type must be mediated via a different mechanism, for example, by activation of Stat3 (47) and a nonspecific cation channel (36) (Figure 11).

In adult PPKO mice, hyperphagia was abolished by central administration of tolbutamide, indicating that hyperphagia in these mice is the consequence of K_{ATP} channel activation in POMC neurons in vivo. The finding that this treatment did not affect food intake in control mice might be explained by the fact that K_{ATP} channels seemed to be largely closed in control mice and, correspondingly, tolbutamide caused only a small increase in firing rate in POMC neurons of control mice (Table 3). Our results also show that in POMC neurons insulin was able, via activation of K_{ATP} channels, to occlude the effects of leptin. Because insulin is anorexigenic, this must mean that it exerts effects on other hypothalamic neurons, which counteract its action on POMC neurons.

Taken together, our results assign K_{ATP} channel activity in POMC neurons a critical role in regulating the set point of hypothalamic POMC cell activity. Apparently, signals strongly stimulating PI3K activate this channel via reduction of sensitivity to ATP. By contrast, glucose has been shown to reduce K_{ATP} conductance via generation of ATP (44), thus increasing electrical activity of the cell. As K_{ATP} channels are regulated by multiple signaling pathways, integration of these different modulators ultimately determines the activity of the melanocortin system. In conclusion, whatever the extent to which individual hormones contribute to PI3K activation, our data clearly demonstrate that precise control of PIP_3 formation and K_{ATP} channel activity in POMC neurons is crucial

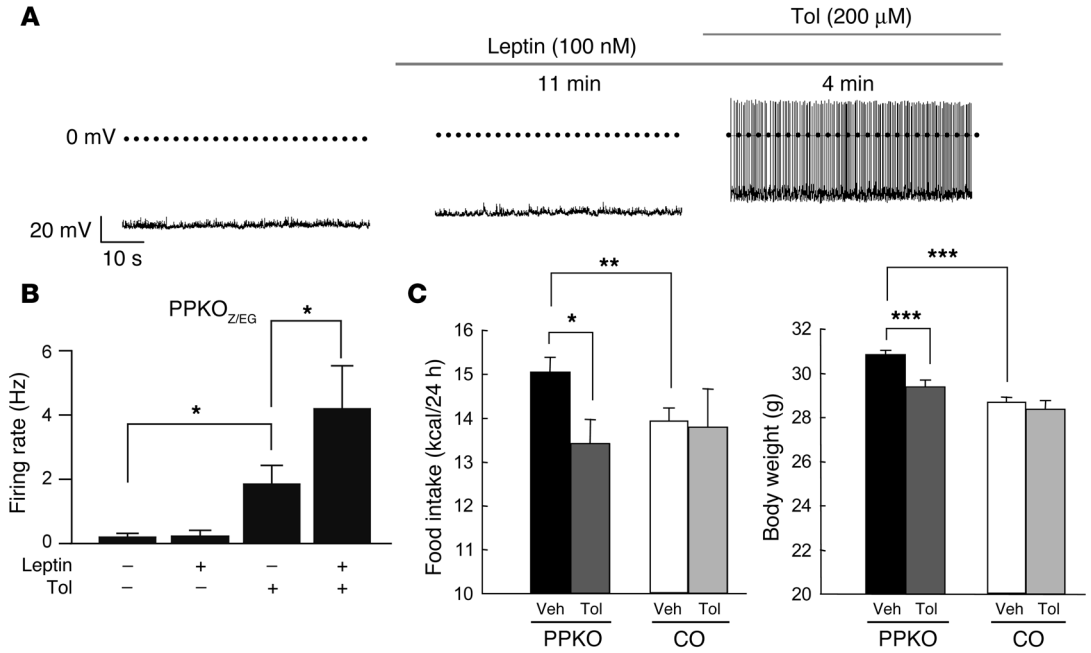

Figure 9
Effect of leptin and tolbutamide (Tol) on electrical activity of PPKO$_{Z/EG}$ POMC neurons and on food intake in vivo. (**A**) Representative membrane potential recording from an identified POMC neuron in an ARC slice from a PPKO$_{Z/EG}$ POMC neuron in the absence of drug, 11 minutes after addition of 100 nM leptin, and 4 minutes after addition of 100 nM leptin plus 200 μM tolbutamide. Note the small depolarization but absence of action potentials produced by leptin alone. A depolarization of similar magnitude (mean depolarization from –58 ± 3 mV to –54 ± 2 mV) was observed in 6 of 9 neurons tested. In the other 3 neurons, leptin caused a small hyperpolarization (from –61 ± 2 mV to –66 ± 3 mV). (**B**) Mean action potential frequency of PPKO$_{Z/EG}$ POMC neurons in the absence of drug and after incubation with leptin and/or tolbutamide (n = 6 per group). (**C**) Food intake and body weight of 15-week-old ND-fed control (n = 4–6) and PPKO (n = 5–9) males after icv administration of either vehicle (Veh) or tolbutamide. Injection of vehicle did not alter food intake in PPKO or control mice compared with uninjected mice (data not shown). Values are mean ± SEM. *$P \leq 0.05$; **$P \leq 0.01$; ***$P \leq 0.001$.

for the maintenance of energy homeostasis. Further exploration of this pathway, which acts independently of that leading to Stat3 phosphorylation, may help to define novel approaches to treatment of obesity and diabetes.

Methods

Animal care. Care of all animals was within institutional animal care committee guidelines. All animal procedures were conducted in compliance with protocols and approved by local government authorities (Bezirksregierung Köln, Cologne, Germany) and were in accordance with NIH guidelines. Mice were housed in groups of 3–5 at 22–24°C using a 12-hour light/12-hour dark cycle. Animals were either fed normal chow (Teklad Global Rodent 2018; Harlan) containing 53.5% carbohydrates, 18.5% protein, and 5.5% fat (12% of calories from fat) or a HFD (C1057; Altromin) containing 32.7% carbohydrates, 20% protein, and 35.5% fat (55.2% of calories from fat). Animals had ad libitum access to water at all times, and food was only withdrawn if required for an experiment. Body weight was measured once a week; body length (naso-anal length) was measured once at week 20, and BMI was calculated as body weight in grams divided by the square of the body length in centimeters (g/cm^2). Genotyping was performed by PCR, using genomic DNA isolated from tail tips as previously described (14, 27). At the end of the study period of 20 weeks, the animals were sacrificed in isoflurane anesthesia.

Generation of PomcCre-Pten$^{lox/lox}$ mice. *PomcCre* mice were mated with *Pten$^{lox/lox}$* mice, and a breeding colony was maintained by mating *Pten$^{lox/lox}$* with *PomcCre-Pten$^{lox/lox}$* mice. *Pten^{lox}* mice had been backcrossed for at least 5 generations on a C57BL/6 background, and *PomcCre* mice — initially established on an FVB background — had been backcrossed for 2 generations on a C57BL/6 background before intercrossing them with *Pten^{lox}* mice. Only animals from the same mixed background strain generation were compared with each other. All stated phenotypes were stable over at least 4 generations.

Restraint stress. Mice were familiarized with gentle handling for approximately 8 weeks prior to the experiment. For determination of basal serum corticosterone levels, blood was drawn from the tail vein during the first 3 hours of the light phase. The following day, mice were subjected to 1 hour of restraint stress at the same time of the light phase. Restraint stress was achieved by enclosing the animals in a plastic tube with a diameter of 3 cm and openings at both ends for tail and nose. The length of the tube was adjusted to the size of the animal to ensure complete immobilization. At the end of the experiment, blood samples were again drawn from the tail vein.

Food intake, indirect calorimetry, physical activity and body core temperature determination. Food intake was measured over 3 weeks, and daily food intake was calculated as the average intake of chow within the time stated. All other measurements were performed with a Comprehensive Laboratory Animal Monitoring System (CLAMS, Oxymax Windows 3.0.3; Columbus Instruments). Chemically disinfected transmitters (PDT-4000 E-Mitter, VitalView Data Acquisition System 4.1; Mini Mitter) were implanted into the peritoneal cavity of mice, which had been anesthetized by intraperitoneal injection of avertin (2,2,2-tribromoethanol and *tert*-amyl alcohol; Sigma-Aldrich). Adequacy of the anesthesia was ensured by the loss of pedal reflexes. After a recovery period of 7 days, only mice that had reached at least 90% of their presurgical body weight were placed at room temperature (22–24°C) in 3.0-l chambers of the CLAMS open-circuit calo-

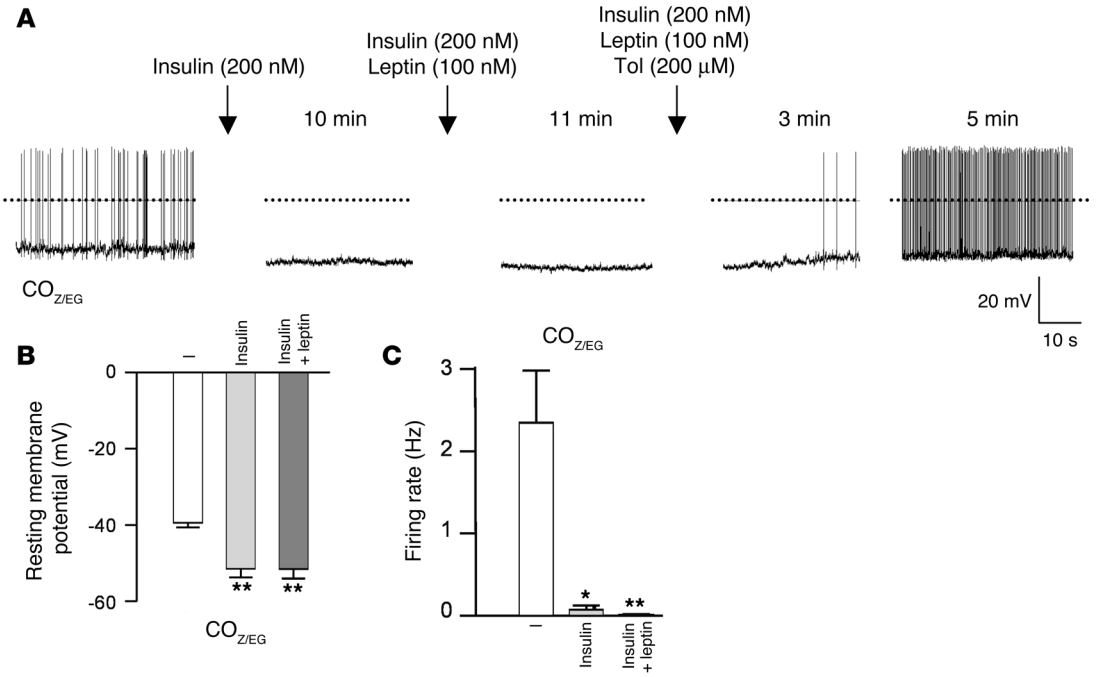

Figure 10
Insulin action in POMC neurons. (**A**) Representative membrane potential recording from an identified POMC neuron in an ARC slice from a $CO_{Z/EG}$ mouse in the absence of drug, 10 minutes after addition of 200 nM insulin, after subsequent addition of 100 nM leptin, and 3 and 5 minutes after addition of 200 μM tolbutamide. Note that the ability of leptin to enhance electrical activity of POMC neurons (35) was blocked when insulin was present, but was restored when the K_{ATP} channel blocker tolbutamide was added to the medium. (**B** and **C**) Mean resting membrane potential (**B**) and mean action potential frequency (**C**) of $CO_{Z/EG}$ POMC neurons in the absence of drug (–), after exposure to 200 nM insulin, and after subsequent addition of 100 nM leptin (n = 3–5). Values are mean ± SEM. $^*P \leq 0.05$; $^{**}P \leq 0.01$.

rimetry. Settling time was set at 150 s, and measuring time was set as at 60 s, with room air as reference. Food and water were provided ad libitum in the appropriate devices. Mice were allowed to acclimatize in the chambers for 24 hours. Locomotor activity, body temperature, and parameters of indirect calorimetry were measured for at least the following 72 hours. Presented data are mean values obtained in these recordings.

Leptin sensitivity was examined by intraperitoneally injecting female control and PPKO mice at the age of 10 weeks that had been exposed to HFD for 7 weeks, or male control and PPKO mice at the age of 15 weeks that had been exposed to ND for 12 weeks, with a leptin dose of 2 mg/kg twice daily over a period of 3 consecutive days. Body weight was determined daily, and food intake was measured continuously in the CLAMS during the experiment.

Determination of body composition. Anesthetized 19-week-old male mice on ND were placed on transparent paper, their extremities were fixed in position with tape, and body composition was determined by dual-energy X-ray absorptiometry with a direct digital densitometry system (LUNAR Prodigy Advance; GE Healthcare).

Intracerebroventricular experiments. For icv cannula implantation, 15-week-old male control and PPKO mice were anesthetized as previously described and placed in a stereotactic device. A sterile osmotic pump connector cannula (Bilaney) was implanted into the left lateral brain ventricle (–0.2 mm anterior and 1.0 mm lateral relative to Bregma and 2.3 mm below the surface of the skull). The support plate of the catheter was attached to the skull with Super Glue (Super Glue Corp.). The catheter was prefilled with artificial cerebrospinal fluid (aCSF; 150 mM Na, 3 mM K, 1.4 mM Ca, 0.8 mM Mg, 1.0 mM P, and 155 mM Cl) and connected to a sealed microrenathane catheter (MRE-025; Braintree Scientific Inc.).

After 5 days of recovery, the sealed microrenathane catheter was removed. Over 1 minute, tolbutamide (30 nmol; Sigma-Aldrich) or vehicle (aCSF, 5% DMSO) was injected, and 1 μl of vehicle was postinjected to assure complete drug administration to the brain. The catheter was subsequently sealed to avoid backflow. Injections were performed in isoflurane anesthesia 1 hour before the onset of the dark cycle. Body weight and food intake were measured every 12 hours under basal/vehicle conditions and after injection of the drug. Correct positioning of the icv cannula was verified in each animal by injection of methylen blue (1%) after sacrificing the mice.

Western blot analysis. Tissues were removed and homogenized in homogenization buffer with a polytron homogenizer, and Western blot analyses were performed as previously described (48) with antibodies raised against Pten (catalog no. MS1250P; Lab Vision) and insulin receptor β subunit (catalog no. sc-711; Santa Cruz Biotechnology Inc.) as loading control.

Hypothalamic neuropeptide expression. Neuropeptide mRNA was analyzed using quantitative RT-PCR. RNA was extracted from hypothalamic blocks using the RNeasy Mini Kit (QIAGEN). Hypothalamic RNA was reversely transcribed with SuperScript Reverse Transcriptase (Invitrogen) and amplified using TaqMan Universal PCR Master Mix, NO AmpErase UNG with TaqMan Assay-on-Demand kits (Applied Biosystems), with the exception of the detection of POMC mRNA, which was performed with customized primers for POMC: sense, 5′-GACACGTGGAAGATGCCGAG-3′; antisense, 5′-CAGCGAGAGGTCGAGTTTGC-3′; probe sequence, 5′-FAM-CAACCTGCTGGCTTGCATCCGG-TAMRA-3′. Relative expression of neuropeptide mRNA was determined using standard curves based on hypothalamic cDNA, and samples were adjusted for total RNA content by TATA box–binding protein RNA quantitative PCR. Calculations were performed by a comparative cycle threshold (Ct) method: the starting copy number of test samples was

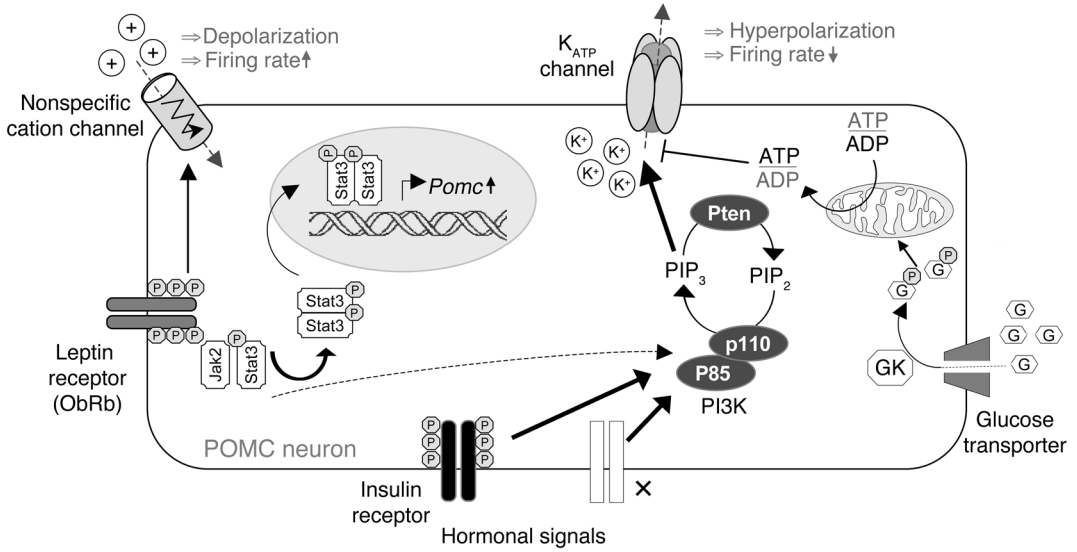

Figure 11
Proposed model of insulin and leptin action in POMC neurons. Insulin hyperpolarizes POMC neurons via robust (solid line) activation of PI3K (p85, regulatory subunit; p110, catalytic subunit) and generation of PIP_3. PIP_3 activates K_{ATP} channels, resulting in hyperpolarization and a decreased neuronal firing rate. By contrast, leptin depolarizes POMC neurons, probably by opening nonspecific cation channels (36). Activation of the leptin receptor produces relatively weak (dashed line) stimulation of PI3K via IRS proteins but strong Stat3 phosphorylation via activation of Jak2, thereby leading to increased expression of POMC. K_{ATP} channel activity is also regulated by metabolically generated ATP and adenosine diphosphate (ADP) (44). This has been proposed to play a role in sensing ambient glucose concentrations (56), thereby regulating neuroendocrine sensitivity to glucose and metabolic efficiency (57). Other hormonal receptors that activate the PI3K pathway are shown by an ×. G^P, glucose-6-phosphate; GK, glucokinase; PIP_2, phosphatidylinositol$_{4,5}$-biphosphate.

determined in comparison with the known copy number of the calibrator sample (ddCt). The relative gene copy number was calculated as 2^{-ddCt}. Quantitative PCR was performed on an ABI-PRISM 7700 Sequence Detector (Applied Biosystems). Assays were linear over 4 orders of magnitude.

Analytical procedures. Blood glucose values were determined from whole venous blood using an automatic glucose monitor (GlucoMen^R *GlycÓ*; A. Menarini Diagnostics). Insulin, leptin, adiponectin, and corticosterone levels in serum were measured by ELISA using mouse standards according to the manufacturer's guidelines (Mouse Leptin ELISA, Mouse/Rat Insulin ELISA; Crystal Chem Inc.; Mouse Adiponectin ELISA, B-Bridge/Correlate-EIA corticosterone Kit; Assay Designs Inc.).

Tissue preparation for immunocytochemistry and immunocytochemical procedures. *PomcCre-Pten*$^{+/+}$ mice and *PomcCre-Pten*$^{lox/lox}$ mice were mated with *RosaArte1* reporter mice. Male ND-fed reporter mice at the age of approximately 12 weeks were starved overnight, anesthetized, and intravenously injected with either saline or 5 U of human regular insulin (Novo Nordisk) for 10 and 20 minutes. As previously described, peripheral intravenous injection of human regular insulin strongly activates insulin receptor signaling in the brain with a maximum in Akt phosphorylation at 10 minutes and almost basal phosphorylated Akt (pAkt) levels at 20 minutes after the injection, with no effect on blood glucose levels during this time (49). Mice were then perfused transcardially with physiologic saline solution, frozen in tissue-freezing medium (Jung Tissue Freezing Medium; Leica Microsystems) and sectioned on a cryostat. Tissues were either stained with H&E or β-gal (catalog no. 55976; Cappel) and PIP_3 (catalog no. Z-G345; Echelon). Double fluorescence immunostainings were performed as previously described (48).

For quantitative analysis of PIP_3 levels in POMC neurons, a total of 808 LacZ-positive neurons was counted in ARC slices of independent control (n = 3; 405 POMC neurons) and PPKO mice (n = 3; 403 POMC neurons), and the amount of PIP_3 was classified as either low (immunoreactive cytoplasmatic dots/sprinkles in the proximity of the nucleus at background levels, i.e., 6 or fewer dots, no cloudy aspect, no confluent areas), moderate (dots/sprinkles at levels above background, i.e., more than 6 dots, cloudy aspect), or high (numerous dots/sprinkles, cloudy with confluent areas) (see Figure 1D). Slides were viewed through a Zeiss Axioskop equipped with a Zeiss AxioCam for acquisition of digital images. Neurons positive for β-gal were counted and marked digitally to prevent multiple counts, and PIP_3 immunoreactivity was rated as described above using Zeiss AxioVision version 4.2 imaging software. Results were expressed as percentage of POMC neurons, which show the respective PIP_3 levels.

POMC cell counts and leptin-stimulated Stat3 phosphorylation. Male 12- to 15-week-old reporter mice on ND were intravenously injected with either saline or 20 μg leptin and anesthetized after 30 minutes. Mice were then perfused transcardially with saline followed by fixation solution containing 4% paraformaldehyde. Hypothalami were dissected, postfixed in fixation solution at 4°C overnight, and soaked in 20% sucrose solution for cryoprotection overnight. Cryoprotected tissues were frozen on dry ice and cut into 30-μm coronal sections on a sliding microtome, collected in 4 series, and stored in antifreeze solution (50% PBS, 15% ethyl glycol, and 35% glycerol) at –20°C until further use. For double labeling of pStat3 and β-gal (indicating POMC-expressing neurons), free-floating tissue sections were extensively washed to remove cryoprotectant, pretreated with 100% methanol precooled to 20°C, and incubated for 20 minutes at room temperature in 0.3% glycine in PBS for 10 minutes and 0.03% SDS in PBS for 10 minutes, including PBS washes during the steps. Subsequently, sections were blocked for 1 hour (3% normal donkey serum in PBS, 0.4% Triton X-100, 0.2% sodium azide) followed by incubation of the primary antibodies, rabbit anti-pStat3 (diluted 1:3,000 in blocking solution; Cell Signalling Technology) and goat anti–β-gal (diluted 1:3,000 in blocking solution; Biogenesis), for 48 hours at 4°C. Sections were extensively washed in PBS,

incubated in darkness for 2 hours at room temperature in anti-rabbit–Alexa 488 (Invitrogen) for labeling of pStat3 antibodies and biotinylated anti-goat antibody (Jackson ImmunoResearch Laboratories Inc.) for detection of β-gal antibodies (both diluted 1:200 in blocking solution without sodium azide). The biotinylated anti-goat antibody was then further labeled with Alexa 568–conjugated streptavidin (diluted 1:200; Invitrogen) for 1 hour in the dark at room temperature. Sections were mounted onto gelatine-coated slides, dried, and coverslipped using mounting media (ProLong Gold; Invitrogen). Fluorescence signals were detected under a fluorescent microscope (BX-51; Olympus), and representative pictures of the ARC were taken with a digital color camera (DP70; Olympus).

For quantification of β-gal–positive POMC cells, tissues were processed as described above for pStat3/β-gal double immunohistochemistry and stained for β-gal. Pictures from every fourth section throughout the ARC (generally 12–13 adjacent sections, Bregma –1.1 mm to –2.7 mm) were taken, and all sections were allocated in a rostral to caudal manner to visualize the distribution of POMC neurons throughout the ARC. Using Adobe Photoshop software version 8.0, β-gal–positive neurons and β-gal–positive neurons showing pStat3 immunoreactivity were counted and marked digitally to prevent multiple counts as previously described (50). Cell counts were performed in 3–4 animals per group for quantification of β-gal–positive POMC neurons and in 1–8 animals per group for assessment of pStat3 generation. Cell numbers represent every fourth section throughout the ARC. POMC cells were quantified in a subset of the mice used for assessment of pStat3 generation.

α-MSH staining. Female control and PPKO mice (20 weeks old) on HFD were anesthetized and perfused transcardially with 40 ml fixative solution containing 2% paraformaldehyde and 4% acrolein in 0.1 M PBS (pH 7.4). The hypothalami were dissected and soaked in 25% sucrose overnight for cryoprotection, after which 25-μm coronal sections were cut through the PVN and the ARC using a freezing microtome (Leica Microsystems). The sections were collected in PBS (pH 7.4) and treated with 1.0% sodium borohydride for 30 minutes, then 0.5% Triton X-100 in 0.5% H_2O_2 in PBS for 15 minutes and in 2% normal horse serum in PBS to block the nonspecific antibody binding. Following pretreatments, the sections were placed in sheep α-MSH antiserum (gift of J.B. Tatro, New England Medical Center, Boston, Massachusetts, USA) at 1:16,000 dilution for 2 days at 4°C, followed by treatment in Cy3-conjugated donkey anti-sheep IgG (diluted 1:100; Jackson ImmunoResearch Laboratories Inc.) for 2 hours. After rinsing in PBS, the sections were mounted and coverslipped with Vectashield mounting medium (Vector Laboratories). Images were taken with Radiance 2100 confocal microscope (Bio-Rad).

For determination of cell diameters, sections were examined under a Zeiss Axioplan 2 microscope outfitted with fluorescent filters, an AxioCam HRc camera, and Axiovision version 4.2 imaging software. Digital color images of the immunofluorescent labeled cells were captured at a magnification of ×100, with a scale bar representing 10 μm applied to each. The images (saved in .TIF format) were then converted to grayscale by means of Adobe Photoshop. Using Scion Image software (Scion Corp.), and with the operator blinded to the experimental conditions, measurements (in μm) of the diameter of each labeled cell were taken. Only those cells that were clearly in the plane of focus and exhibited a distinct nucleus and well-defined cell outline were selected. The measurement was taken across the widest extent of the cell and always crossed the nucleus.

For quantification of α-MSH in projecting fibers, free-floating brain sections (50 μm) containing the PVN were immunostained for POMC (β-endorphin) by our standard protocol (51) using diaminobenzidine as the chromagen. Sections were examined under a Zeiss Axioplan 2 microscope equipped with a motorized stage, Stereo Investigator software for Design Based Stereology (MicroBrightField Inc.), and a Microfire camera from Optronics. Every section containing the PVN (n = 3) was examined for each animal, with the operator blinded to the experimental conditions. For each hemisphere of the PVN, at a magnification of ×63, a single plane of focus was chosen and captured; an outline (kept consistent between hemispheres and sections) was drawn around the PVN. The fractionator function was selected in order to accomplish a stereological analysis of a 2-dimensional image. Briefly, a lattice (of known size, i.e., the sampling area) was randomly placed over the delineated region of interest by the computer program. A counting frame of known size (square frame with 2 sides outlined in green and 2 sides in red) was placed at every x and y intersection of the lattice that was located on the area of interest. Fibers were counted if they were within the counting frame or touched the green lines; they were excluded if they intersected the red lines or fell outside of the counting frame. A calculation of the total number of markers counted per the entire sampling area was recorded and compared between groups.

Ultrastructural analysis of POMC perikarya. Female control and PPKO mice on HFD (11 weeks old) were anesthetized and perfused transcardially with saline followed by 100 ml Somogyi-Takagi fixative containing 4% paraformaldehyde and 0.8% glutaraldehyde in 0.1 M phosphate buffer (PB). The brains were dissected and postfixed in glutaraldehyde-free fixative solution for at least 2 hours at 4°C and washed in 0.1 M PB. Tissue blocks containing the ARC were dissected from each brain. Vibratome sections (50 μm) were cut and washed in 0.1 M PB. To eliminate unbound aldehydes, sections were incubated in 1% sodium borohydride for 15 minutes, then rinsed in PB. Subsequently, sections were incubated in rabbit anti-POMC antisera (diluted 1:3,000 in PB; refs. 51, 52) for 24 hours at room temperature followed by incubation in biotinylated goat anti-rabbit immunoglobulin (diluted 1:250; Vector Laboratories) for 2 hours at room temperature. Sections were then incubated in avidin-biotin complex (2 hours at room temperature, ABC Elite Kit; Vector Laboratories), and the tissue-bound peroxidase was visualized by a diaminobenzidine reaction. After immunostaining, the sections were osmicated (15 minutes in 1% osmium tetroxide in PB) and dehydrated in increasing ethanol concentrations. During the dehydration, 1% uranyl acetate was added to the 70% ethanol to enhance ultrastructural membrane contrast. Dehydration was followed by flat-embedding in Araldite. Ultrathin sections were cut on a Leica ultra microtome, collected on Formvar-coated single-slot grids, and analyzed with a Tecnai 12 Biotwin (FEI Company) electron microscope. Only POMC-immunolabeled cells with equal immunoperoxidase density were studied.

Electrophysiology. Coronal brain slices (250–300 μm) containing the ARC were prepared from 10- to 16-day-old female and male $CO_{Z/EG}$ and $PPKO_{Z/EG}$ mice as previously described (53). After at least 15 minutes' recovery at 35°C in aCSF gassed with 95% O_2 and 5% CO_2, brain slices were transferred to a recording chamber continuously perfused at 2–4 ml/min with gassed aCSF (125 mM NaCl; 21 mM $NaHCO_3$; 2.5 mM KCl; 1.2 mM NaH_2PO_4; 10 mM HEPES; 2 mM $CaCl_2$; 2 mM $MgCl_2$; 5 mM glucose, pH 7.4; and 200 μM tolbutamide where indicated in Figures 7, 9, and 10). Patch pipettes were filled with internal solution containing 128 mM K-gluconate, 10 mM KCl, 10 mM HEPES, 0.1 mM EGTA, 2 mM $MgCl_2$, 0.3 mM Na-GTP, and 3 mM K_2-ATP, pH 7.3 adjusted with KOH. Experiments were carried out at 22–25°C.

Brain slices were viewed with a Zeiss Axioskop fitted with fluorescence and infrared differential interference contrast (IR-DIC) videomicroscopy. Fluorescent POMC-EGFP neurons were identified by epifluoresecnce and patched under IR-DIC optics. Whole-cell recordings were made using an EPC-9 patch-clamp amplifier. Patch pipettes had resistances of 3–5 MΩ when filled with internal solution.

Data were filtered, sampled with Pulse/Pulsefit and software (Heka Electronik) and analyzed with Pulsefit 8.67 and Origin 6.0 software (MicroCal). Most $PPKO_{Z/EG}$ POMC neurons were hyperpolarized, and fired at a much

lower frequency than $CO_{Z/EG}$ or were electrically silent (Table 2). Four neurons of 16, however, were not hyperpolarized and had a firing frequency similar to that of $CO_{Z/EG}$ neurons (mean 5.2 ± 2.3 Hz). These data are consistent with previous findings that approximately 25% of hypothalamic POMC neurons do not express K_{ATP} channels (34). Resting potential was measured by displaying the traces on a very long time scale, when a clear basal line became evident. Firing frequency was determined by counting the number of action potentials within 1-minute sweeps (usually 3 were averaged). Membrane conductance was measured by applying a voltage ramp (70 mV/s) from –100 mV to –30 mV from a holding potential of –60 mV and fitting the current between –70 and –95 mV with a straight line.

We quantified the K_{ATP} conductance by measuring the difference in membrane conductance in the presence and absence of 200 μM tolbutamide (Table 2), a concentration that blocks K_{ATP} currents by >95% (54). Currents and conductances were normalized to cell capacitance to correct for differences in cell size because $PPKO_{Z/EG}$ neurons were significantly larger than $CO_{Z/EG}$ neurons (9 versus 25 pF; Table 3). Thus conductance was normalized to cell capacitance to correct differences in cell size. The larger size is consistent with the known effect of PIP_3 on growth (55). Because electrical activity in both control and PPKO mice was the same in male and female animals (Table 1), we merged the data from males and females in subsequent experiments.

Statistics. Data sets were analyzed for statistical significance using a 2-tailed unpaired Student's *t* test. *P* values less than 0.05 were considered significant.

Acknowledgments

We wish to thank Gisela Schmall for excellent secretarial assistance and Julia Baumgartl and Sigrid Irlenbusch for outstanding technical assistance. We thank Bradford Lowell and Joel Elmquist for kindly providing the Pomc-Cre mice. This work was supported by the Köln Fortune Program (132/2003 and 159/2004 to L. Plum) as well as by grants from the Bundesministerium für Bildung, Wissenschaft, Forschung, und Technologie (BMBF; ZMMKTV2 to W. Krone and J.C. Brüning), the European Union (LSHM-CT-2003-503041 to J.C. Brüning), Thyssen Stiftung (10.04.1.153 to J.C. Brüning), the Wellcome Trust (to F.M. Ashcroft), the Royal Society (to F.M. Ashcroft and D. Burdakov), the American Heart Association (AHA0535298N to H. Münzberg), and the NIH (DK-060711 and RR-014451 to T.L. Horvath).

Received for publication October 12, 2005, and accepted in revised form May 9, 2006.

Address correspondence to: Jens C. Brüning, Institute for Genetics, Department of Mouse Genetics and Metabolism, Zülpicher Straβe 47, 50674 Köln, Germany. Phone: 49-221-470-2467; Fax: 49-221-470-5185; E-mail: jens.bruening@uni-koeln.de.

Leona Plum and Xiaosong Ma contributed equally to this work.

1. Mokdad, A.H., et al. 2001. The continuing epidemics of obesity and diabetes in the United States. *JAMA.* **286**:1195–1200.
2. Halaas, J.L., et al. 1995. Weight-reducing effects of the plasma protein encoded by the obese gene. *Science.* **269**:543–546.
3. Polonsky, K.S., Given, B.D., and Van Cauter, E. 1988. Twenty-four-hour profiles and pulsatile patterns of insulin secretion in normal and obese subjects. *J. Clin. Invest.* **81**:442–448.
4. Polonsky, K.S., et al. 1988. Quantitative study of insulin secretion and clearance in normal and obese subjects. *J. Clin. Invest.* **81**:435–441.
5. Bagdade, J.D., Bierman, E.L., and Porte, D., Jr. 1967. The significance of basal insulin levels in the evaluation of the insulin response to glucose in diabetic and nondiabetic subjects. *J. Clin. Invest.* **46**:1549–1557.
6. Havrankova, J., Roth, J., and Brownstein, M. 1978. Insulin receptors are widely distributed in the central nervous system of the rat. *Nature.* **272**:827–829.
7. Margolis, R.U., and Altszuler, N. 1967. Insulin in the cerebrospinal fluid. *Nature.* **215**:1375–1376.
8. Air, E.L., Benoit, S.C., Clegg, D.J., Seeley, R.J., and Woods, S.C. 2002. Insulin and leptin combine additively to reduce food intake and body weight in rats. *Endocrinology.* **143**:2449–2452.
9. van Houten, M., Posner, B.I., Kopriwa, B.M., and Brawer, J.R. 1979. Insulin-binding sites in the rat brain: in vivo localization to the circumventricular organs by quantitative radioautography. *Endocrinology.* **105**:666–673.
10. Schwartz, M.W., Seeley, R.J., Campfield, L.A., Burn, P., and Baskin, D.G. 1996. Identification of targets of leptin action in rat hypothalamus. *J. Clin. Invest.* **98**:1101–1106.
11. Benoit, S.C., et al. 2002. The catabolic action of insulin in the brain is mediated by melanocortins. *J. Neurosci.* **22**:9048–9052.
12. Baskin, D.G., Breininger, J.F., and Schwartz, M.W. 1999. Leptin receptor mRNA identifies a subpopulation of neuropeptide Y neurons activated by fasting in rat hypothalamus. *Diabetes.* **48**:828–833.
13. Cheung, C.C., Clifton, D.K., and Steiner, R.A. 1997. Proopiomelanocortin neurons are direct targets for leptin in the hypothalamus. *Endocrinology.* **138**:4489–4492.
14. Balthasar, N., et al. 2004. Leptin receptor signaling in POMC neurons is required for normal body weight homeostasis. *Neuron.* **42**:983–991.
15. Plum, L., Schubert, M., and Bruning, J.C. 2005. The role of insulin receptor signaling in the brain. *Trends Endocrinol. Metab.* **16**:59–65.
16. Schwartz, M.W., and Porte, D., Jr. 2005. Diabetes, obesity, and the brain. *Science.* **307**:375–379.
17. Gropp, E., et al. 2005. Agouti-related peptide-expressing neurons are mandatory for feeding. *Nat. Neurosci.* **8**:1289–1291.
18. Sipols, A.J., Baskin, D.G., and Schwartz, M.W. 1995. Effect of intracerebroventricular insulin infusion on diabetic hyperphagia and hypothalamic neuropeptide gene expression. *Diabetes.* **44**:147–151.
19. Schwartz, M.W., et al. 1992. Inhibition of hypothalamic neuropeptide Y gene expression by insulin. *Endocrinology.* **130**:3608–3616.
20. Seeley, R.J., et al. 1997. Melanocortin receptors in leptin effects [letter]. *Nature.* **390**:349.
21. Bousquet, C., Zatelli, M.C., and Melmed, S. 2000. Direct regulation of pituitary proopiomelanocortin by STAT3 provides a novel mechanism for immuno-neuroendocrine interfacing. *J. Clin. Invest.* **106**:1417–1425.
22. Kim, Y.B., Uotani, S., Pierroz, D.D., Flier, J.S., and Kahn, B.B. 2000. In vivo administration of leptin activates signal transduction directly in insulin-sensitive tissues: overlapping but distinct pathways from insulin. *Endocrinology.* **141**:2328–2339.
23. Backer, J.M., et al. 1992. Phosphatidylinositol 3′-kinase is activated by association with IRS-1 during insulin stimulation. *EMBO J.* **11**:3469–3479.
24. Niswender, K.D., et al. 2001. Intracellular signalling. Key enzyme in leptin-induced anorexia. *Nature.* **413**:794–795.
25. Niswender, K.D., et al. 2003. Insulin activation of phosphatidylinositol 3-kinase in the hypothalamic arcuate nucleus: a key mediator of insulin-induced anorexia. *Diabetes.* **52**:227–231.
26. Xu, A.W., et al. 2005. PI3K integrates the action of insulin and leptin on hypothalamic neurons. *J. Clin. Invest.* **115**:951–958. doi:10.1172/JCI200524301.
27. Suzuki, A., et al. 2001. T cell-specific loss of Pten leads to defects in central and peripheral tolerance. *Immunity.* **14**:523–534.
28. Wang, J., et al. 2001. Overfeeding rapidly induces leptin and insulin resistance. *Diabetes.* **50**:2786–2791.
29. Khan, F.A., Goforth, P.B., Zhang, M., and Satin, L.S. 2001. Insulin activates ATP-sensitive K(+) channels in pancreatic beta-cells through a phosphatidylinositol 3-kinase-dependent pathway. *Diabetes.* **50**:2192–2198.
30. Harvey, J., Hardy, S.C., Irving, A.J., and Ashford, M.L. 2000. Leptin activation of ATP-sensitive K+ (KATP) channels in rat CRI-G1 insulinoma cells involves disruption of the actin cytoskeleton. *J. Physiol.* **527**:95–107.
31. Mirshamsi, S., et al. 2004. Leptin and insulin stimulation of signalling pathways in arcuate nucleus neurones: PI3K dependent actin reorganization and KATP channel activation. *BMC Neurosci.* **5**:54.
32. Spanswick, D., Smith, M.A., Groppi, V.E., Logan, S.D., and Ashford, M.L. 1997. Leptin inhibits hypothalamic neurons by activation of ATP-sensitive potassium channels. *Nature.* **390**:521–525.
33. Ashcroft, S.J., and Ashcroft, F.M. 1990. Properties and functions of ATP-sensitive K-channels. *Cell. Signal.* **2**:197–214.
34. Ibrahim, N., et al. 2003. Hypothalamic proopiomelanocortin neurons are glucose responsive and express K(ATP) channels. *Endocrinology.* **144**:1331–1340.
35. Choudhury, A.I., et al. 2005. The role of insulin receptor substrate 2 in hypothalamic and β cell function. *J. Clin. Invest.* **115**:940–950. doi:10.1172/JCI200524445.
36. Cowley, M.A., et al. 2001. Leptin activates anorexigenic POMC neurons through a neural network in the arcuate nucleus. *Nature.* **411**:480–484.
37. Novak, A., Guo, C., Yang, W., Nagy, A., and Lobe, C.G. 2000. Z/EG, a double reporter mouse line that expresses enhanced green fluorescent protein upon Cre-mediated excision. *Genesis.* **28**:147–155.
38. Shyng, S.L., and Nichols, C.G. 1998. Membrane phospholipid control of nucleotide sensitivity of KATP channels. *Science.* **282**:1138–1141.
39. Cabrele, C., and Beck-Sickinger, A.G. 2000. Molecular characterization of the ligand-receptor interaction of the neuropeptide Y family. *J. Pept. Sci.* **6**:97–122.

40. Clegg, D.J., Riedy, C.A., Smith, K.A., Benoit, S.C., and Woods, S.C. 2003. Differential sensitivity to central leptin and insulin in male and female rats. *Diabetes.* **52**:682–687.
41. Bruning, J.C., et al. 2000. Role of brain insulin receptor in control of body weight and reproduction. *Science.* **289**:2122–2125.
42. Alfadda, A., DosSantos, R.A., Stepanyan, Z., Marrif, H., and Silva, J.E. 2004. Mice with deletion of the mitochondrial glycerol-3-phosphate dehydrogenase gene exhibit a thrifty phenotype: effect of gender. *Am. J. Physiol. Regul. Integr. Comp. Physiol.* **287**:R147–R156.
43. Lewitt, M.S., and Brismar, K. 2002. Gender difference in the leptin response to feeding in peroxisome-proliferator-activated receptor-alpha knockout mice. *Int. J. Obes. Relat. Metab. Disord.* **26**:1296–1300.
44. MacGregor, G.G., et al. 2002. Nucleotides and phospholipids compete for binding to the C terminus of KATP channels. *Proc. Natl. Acad. Sci. U. S. A.* **99**:2726–2731.
45. Kwon, C.H., et al. 2001. Pten regulates neuronal soma size: a mouse model of Lhermitte-Duclos disease. *Nat. Genet.* **29**:404–411.
46. Huang, H., et al. 1999. PTEN affects cell size, cell proliferation and apoptosis during Drosophila eye development. *Development.* **126**:5365–5372.
47. Bates, S.H., et al. 2003. STAT3 signalling is required for leptin regulation of energy balance but not reproduction. *Nature.* **421**:856–859.
48. Schubert, M., et al. 2004. Role for neuronal insulin resistance in neurodegenerative diseases. *Proc. Natl. Acad. Sci. U. S. A.* **101**:3100–3105.
49. Freude, S., et al. 2005. Peripheral hyperinsulinemia promotes tau phosphorylation in vivo. *Diabetes.* **54**:3343–3348.
50. Munzberg, H., Flier, J.S., and Bjorbaek, C. 2004. Region-specific leptin resistance within the hypothalamus of diet-induced obese mice. *Endocrinology.* **145**:4880–4889.
51. Horvath, T.L., Naftolin, F., and Leranth, C. 1992. GABAergic and catecholaminergic innervation of mediobasal hypothalamic beta-endorphin cells projecting to the medial preoptic area. *Neuroscience.* **51**:391–399.
52. Horvath, T.L., Diano, S., and van den Pol, A.N. 1999. Synaptic interaction between hypocretin (orexin) and neuropeptide Y cells in the rodent and primate hypothalamus: a novel circuit implicated in metabolic and endocrine regulations. *J. Neurosci.* **19**:1072–1087.
53. Burdakov, D., and Ashcroft, F.M. 2002. Cholecystokinin tunes firing of an electrically distinct subset of arcuate nucleus neurons by activating A-Type potassium channels. *J. Neurosci.* **22**:6380–6387.
54. Trube, G., Rorsman, P., and Ohno-Shosaku, T. 1986. Opposite effects of tolbutamide and diazoxide on the ATP-dependent K+ channel in mouse pancreatic beta-cells. *Pflugers Arch.* **407**:493–499.
55. Goberdhan, D.C., Paricio, N., Goodman, E.C., Mlodzik, M., and Wilson, C. 1999. Drosophila tumor suppressor PTEN controls cell size and number by antagonizing the Chico/PI3-kinase signaling pathway. *Genes Dev.* **13**:3244–3258.
56. Levin, B.E., Dunn-Meynell, A.A., and Routh, V.H. 2001. Brain glucosensing and the K(ATP) channel. *Nat. Neurosci.* **4**:459–460.
57. Mobbs, C.V., et al. 2005. Impaired glucose signaling as a cause of obesity and the metabolic syndrome: the glucoadipostatic hypothesis. *Physiol. Behav.* **85**:3–23.